

Comprehensive Summaries of Uppsala Dissertations  
from the Faculty of Science and Technology 697



# Solar Thermal Collectors at High Latitudes

*Design and Performance of Non-Tracking Concentrators*

BY

MONIKA ADSTEN



ACTA UNIVERSITATIS UPSALIENSIS  
UPPSALA 2002

## ABSTRACT

Adsten, M. 2002. Solar thermal collectors at high latitudes -Design and performance of non-tracking concentrators. Acta Universitatis Upsaliensis. *Comprehensive Summaries of Uppsala Dissertations from the Faculty of Science and Technology* 697. 78 pp. Uppsala. ISBN 91-554-5274-4

Solar thermal collectors at high latitudes have been studied, with emphasis on concentrating collectors. A novel design of concentrating collector, the Maximum Reflector Collector (MaReCo), especially designed for high latitudes, has been investigated optically and thermally. The MaReCo is an asymmetrical compound parabolic concentrator with a bi-facial absorber. The collector can be adapted to various installation conditions, for example stand-alone, roof- or wall mounted. MaReCo prototypes have been built and outdoor-tested. The evaluation showed that all types work as expected and that the highest annually delivered energy output,  $340 \text{ kWh/m}^2$ , is found for the roof MaReCo. A study of the heat-losses from the stand-alone MaReCo lead to the conclusion that teflon transparent insulation should be placed around the absorber, which decreases the U-value by about 30%.

A method was developed to theoretically study the projected radiation distribution incident on the MaReCo bi-facial absorber. The study showed that the geometry of the collectors could be improved by slight changes in the acceptance intervals. It also indicated that the MaReCo design concept could be used also at mid-European latitudes if the geometry is changed.

A novel method was used to perform outdoor measurements of the distribution of concentrated light on the absorber and then to calculate the annually collected zero-loss energy,  $E_{a,corr}$ , together with the annual optical efficiency factor. A study using this method indicated that the absorber should be mounted along the  $20^\circ$  optical axis instead of along the  $65^\circ$  optical axis, which leads to an increase of about 20% in  $E_{a,corr}$ . The same absorber mounting is suggested from heat loss measurements. The  $E_{a,corr}$  at  $20^\circ$  absorber mounting angle can be increased by 5% if the absorber fin thickness is changed from 0.5 to 1 mm and by 13% if two 71.5 mm wide fins are used instead of one that is 143 mm wide. If the  $E_{a,corr}$  for the standard stand-alone MaReCo with 143 mm wide absorber mounted at  $65^\circ$  is compared to that of a collector with a 71.5 mm wide absorber mounted at  $20^\circ$ , the theoretical increase is 38%.

*Monika Adsten, Department of Materials Science, The Ångström Laboratory, Uppsala University, Box 534, SE-751 21 Uppsala, Sweden*

© Monika Adsten 2002

ISSN 1104-232X

ISBN 91-554-5274-4

Printed in Sweden by Uppsala University, Tryck & Medier, Uppsala 2002

*This thesis is based on work conducted within the interdisciplinary graduate school Energy Systems. The national Energy Systems Programme aims at creating competence in solving complex energy problems by combining technical and social sciences. The research programme analyses processes for the conversion, transmission and utilisation of energy, combined together in order to fulfil specific needs.*



The research groups that participate in the Energy Systems Programme are the Division of Solid State Physics at Uppsala University, the Division of Energy Systems at Linköping Institute of Technology, the Department of Technology and Social Change at Linköping University, the Department of Heat and Power Technology at Chalmers Institute of Technology in Göteborg as well as the Division of Energy Processes and the Department of Industrial Information and Control Systems at the Royal Institute of Technology in Stockholm.

## PUBLICATIONS INCLUDED IN THE THESIS

- I. Adsten M., Helgesson A. and Karlsson B. (2001). Evaluation of asymmetric CPC-collector designs for stand-alone, roof- or wall integrated installation, submitted to *Solar Energy*
- II. Adsten M., Wäckelgård E. and Karlsson B. (2002). Calorimetric measurements of heat losses from a truncated asymmetric solar thermal concentrator, Submitted to *Solar Energy*
- III. Adsten M., and Karlsson B. (2002). Annually projected solar radiation distribution analysis for optimum design of asymmetric CPC, submitted to *Solar Energy*
- IV. Adsten M., Hellström B. and Karlsson B. (2001) Measurement of radiation distribution on the absorber in an asymmetric CPC collector, submitted to *Solar Energy*
- V. Adsten M., Hellström B. and Karlsson B. (2002). Comparison of the optical efficiency of a wide and a narrow absorber fin in an asymmetric concentrating collector, in manuscript
- VI. Adsten M., Perers B. and Wäckelgård E. (2002), The influence of climate and location on collector performance, *J. Renewable Energy*, Volume **25**, Issue 4, April 2002, Pages 499-509
- VII. Adsten M. and Perers, B. (1999), Simulation of the influence of tilt and azimuth angles on the collector output of solar collectors at northern latitudes, *Proceedings North Sun conference 1999*, Edmonton Canada
- VIII. Hellström B., Adsten M., Nostell P., Wäckelgård E. and Karlsson B. (2000), The impact of optical and thermal properties on the performance of flat plate solar collectors, *Proceedings Eurosun 2000*, Denmark
- IX. Rönnelid M., Adsten M. Lindström T. Nostell P. and Wäckelgård E. (2001), Optical scattering from rough aluminum surfaces, *J. Applied Optics*, **40**, pp 2148-2158
- X. Adsten M., Joerger R., Järrendahl K. and Wäckelgård E. (2000) Optical characterization of industrially sputtered nickel-nickel oxide solar selective surface, *Solar Energy* **68**, 325-328.

### Comments on my participation

- |       |  |
|-------|--|
| I-VII | Major part of calculations/experimental work and writing |
| VIII  | Part of simulations, part of writing                     |
| IX    | Part of optical measurements and writing                 |
| X     | Part of optical measurements                             |

## **PUBLICATIONS NOT INCLUDED IN THE THESIS**

Wäckelgård E, Adsten M and Joerger R (1998). Optical characterization of industrially sputtered nickel-nickel oxide solar selective surface, *Proceedings of EuroSun 1998*, Portoroz, Slovenia

Adsten M and Wäckelgård E (1999). Solar energy-cost effective for the Navestad residential area, Arbetsnotat nr 6, Program Energisystem, ISSN 1403-8307

Adsten M and Perers B (1999). Influence on solar collector output by annual climate variation, internal report, Uppsala University Department of Materials Science

Adsten M and Perers B (2000). Influence of climate variation on collector output, *Proceedings of World Renewable Conference 2000*, Brighton UK

Adsten M and Karlsson B (2001). Measurement of radiation distribution on the absorber in an asymmetric CPC collector, *Proceedings of ISES Solar World Conference*, Adelaide, Australia

Hellström, B., Adsten, M., Nostell, P., Wäckelgård, E. and Karlsson B. (2002), The impact of optical and thermal properties on the performance of flat plate solar collectors, accepted to *Renewable Energy*

# CONTENTS

1	INTRODUCTION.....	1
2	THEORETICAL BACKGROUND AND EXPERIMENTAL METHODS .....	3
2.1	Collector analysis.....	3
2.1.1	The solar collector.....	3
2.1.2	Introduction to optics.....	4
2.1.3	Introduction to thermal radiation.....	7
2.1.4	Characterisation of solar collector components .....	8
2.1.5	Instruments for optical characterisation .....	13
2.1.6	Collector heat losses.....	14
2.1.7	Characterisation of the collector.....	20
2.2	Collector simulations .....	21
2.2.1	Introduction .....	21
2.2.2	The MINSUN program .....	22
2.3	Optical characteristics of nonimaging concentrating collectors.....	23
2.3.1	Introduction .....	23
2.3.2	Description of the Maximum Reflector Collector, MaReCo .....	25
2.3.3	MaReCo prototypes.....	26
2.3.4	Characterisation of concentration distribution on the absorber fin.....	29
2.3.5	Annually collected energy and optical efficiency factor.....	30
2.4	Projection of solar radiation.....	32
2.4.1	Introduction .....	32
2.4.2	Horizontal system.....	33
2.4.3	Rotated system .....	34
2.4.4	Projection angles .....	35
2.4.5	Radiation distribution diagrams .....	35
3	RESULTS AND DISCUSSION .....	39
3.1	The MaReCo.....	39
3.2	Flat plate collectors.....	52
3.3	Component studies.....	60
4	CONCLUSIONS AND SUGGESTION FOR FUTURE WORK.....	64
5	SUMMARY OF APPENDED PAPERS.....	68
6	ACKNOWLEDGEMENTS .....	73
7	REFERENCES.....	75

# NOMENCLATURE

$A(\lambda, \theta)$	Absorptance at wavelength $\lambda$ and angle $\theta$ [-]
$A_{\text{abs}}$	Area of absorber [ $\text{m}^2$ ]
$A_c$	Collector aperture area [ $\text{m}^2$ ]
$A_i$	Area of surface $i$ [ $\text{m}^2$ ]
$A_s, A_p$	Amplitude of incoming radiation for s- and p polarised light respectively [-]
$b_0$	Incidence angle modifier coefficient [-]
$c$	Speed of light [m/s]
$C_i$	Area concentration [-]
$C_{\text{eff}}$	Effective concentration [-]
$d$	Thickness [m]
$E(\lambda, \theta)$	Emittance at wavelength $\lambda$ and angle $\theta$ [-]
$E_a$	Annually collected zero-loss energy not corrected for $F'c[x]$ [a.u.]
$E_{a,\text{corr}}$	Annually collected zero-loss energy corrected for $F'c[x]$ [a.u.]
$E_{\text{interval}}$	Annual energy available within acceptance interval [ $\text{kWh/m}^2$ ]
$E_{\text{tot}}$	Total annual energy incident on surface [ $\text{kWh/m}^2$ ]
$F'$	Collector efficiency [-]
$F'_{\text{av}}$	Mean temperature collector efficiency factor [-]
$F'_c(x)$	Local optical efficiency factor distribution [-]
$F'_{c,a}$	Annual optical efficiency factor [-]
$F'(\tau\alpha)_b$	Zero Loss efficiency for beam radiation [at normal incidence] [-]
$F'(\tau\alpha)_d$	Zero Loss efficiency for diffuse radiation [in collector plane] [-]
$F'U_{L1}$	First order heat loss coefficient [ $\text{W/m}^2\text{K}$ ]
$F'U_{L2}$	Temperature dependence in heat loss coefficient [ $\text{W/m}^2\text{K}^2$ ]
$\hat{F}_{ij}$	Exchange factor [-]
$F_{12}$	View factor between surfaces 1 and 2 [-]
$G$	Direct solar irradiance [ $\text{kWh/m}^2$ ]
$G(\theta)$	Annually projected solar radiation distribution [-]
$G_b$	Annual beam radiation [ $\text{kWh/m}^2$ ]
$G_d$	Annual diffuse radiation [ $\text{kWh/m}^2$ ]
$G_{\text{total}}$	Annual total radiation [ $\text{kWh/m}^2$ ]
$h$	Planck constant [Js]
$h_{\text{sun}}$	Solar height in the horizontal system [ $^\circ$ ]
$h_1$	Internal convection coefficient [ $\text{W/m}^2\text{K}$ ]
$h_2$	Plate to cover radiation coefficient [ $\text{W/m}^2\text{K}$ ]
$h_3$	External convection coefficient [ $\text{W/m}^2\text{K}$ ]
$h_4$	External radiation coefficient for clear sky conditions [ $\text{W/m}^2\text{K}$ ]
$h_r$	Radiation heat transfer coefficient [ $\text{W/m}^2\text{K}$ ]
$I_b(\lambda, T)$	Blackbody radiation wavelength distribution [-]
$I_b$	Total amount of energy emitted [ $\text{WK}^2/\text{m}^2$ ]
$I_e$	Applied electric current [A]
$I_{\text{sol}}(\lambda)$	Incident solar radiation distribution [ $\text{W/m}^3$ ]
$k$	Extinction coefficient [-]
$k_b$	Boltzmann constant [J/K]
$k_c$	Insulation conductivity [ $\text{W/mC}$ ]
$K_{\tau\alpha}$	Incidence angle modifier [-]
$L$	Insulation thickness [m]
$(\text{mC})_e$	Effective thermal capacity for the collector [ $\text{J/m}^2\text{K}$ ]
$n$	Optical refractive index [-]
$N$	Complex refractive index [-]; number of intervals/surfaces [-]
$q(\theta)$	Collected zero-loss energy not corrected for $F'c[x]$ [a.u.]
$q_{\text{corr}}(\theta)$	Collected zero-loss energy corrected for $F'c[x]$ [a.u.]
$Q_i$	Amount of energy exchanged through radiation by surface $i$ [W]

$q_u$	Useful delivered energy output [kWh/m <sup>2</sup> ]
$Q_u$	Useful delivered energy output [kWh]
$r_s, r_p$	Ratio between reflected and incoming light for s-and p polarised light [-]
$\vec{r}$	Position vector [-]
$R$	Reflectance amplitude [-]
$R(\lambda, \theta)$	Reflectance intensity at wavelength $\lambda$ and angle $\theta$ [-]
$R_s, R_p$	Amplitude of reflected radiation for s- and p polarised light respectively [-]
$R_{sol}$	Solar reflectance [-]
$S$	Radiation absorbed by the collector [kWh/m <sup>2</sup> ]
$\vec{s}$	Unit vector in the direction of the wave propagation [-]
$S_c(x)$	Concentration distribution on the absorber [-]
$t$	Time [s]
$T_a$	Ambient temperature [°]
$T_f$	Mean fluid temperature in the collector [K]
$T_i$	Temperature of surface i [°]
$T_{in}$	Temperature of water out of the collector [°C]
$T_{out}$	Temperature of water into the collector [°C]
$T_{pm}$	Mean absorber plate temperature [°]
$T_{sol}$	Solar transmittance [-]
$T_t(\lambda, \theta)$	Transmittance at wavelength $\lambda$ and angle $\theta$ [-]
$(UA)_{edge}$	Edge loss coefficient-area product [W/K]
$U_b$	Back loss coefficient [W/m <sup>2</sup> C]
$U_e$	Edge loss coefficient [W/m <sup>2</sup> C]
$U_L$	Collector overall heat loss coefficient [W/m <sup>2</sup> C]
$U_L^{lab}$	Laboratory U-value [W/m <sup>2</sup> C]
$U_t$	Top loss coefficient [W/m <sup>2</sup> C]
$U_1$	First order heat loss coefficient [W/m <sup>2</sup> K]
$U_2$	Second order heat loss coefficient [W/m <sup>2</sup> K <sup>2</sup> ]
$V$	Volume [m <sup>3</sup> ]
$V_e$	Applied electric voltage [V]
$x$	Location on absorber [m]
$z_i$	Distance from mean surface level [m]
$\alpha_{sol}$	Solar absorptance of the absorber [-]
$\beta$	Aperture tilt [°]
$\delta$	Phase change [-]
$\delta_{rms}$	rms-value [m]
$\Delta T$	Temperature difference between $T_f$ and ambient temperature [K]
$\epsilon$	Dielectric permeability [-]
$\epsilon_i$	Emittance of surface i [-]
$\epsilon_{therm}$	Thermal emittance [-]
$\phi$	Angle [°]
$\gamma_s$	Solar azimuth [°]
$\eta_{0b}$	Beam zero-loss efficiency [-]
$\eta_{0d}$	Diffuse zero-loss efficiency [-]
$\lambda$	Wavelength [m]
$\mu$	Magnetic permeability [-]
$\theta$	Angle [°]
$\theta_c$	Acceptance half angle [°]
$\theta_l$	Longitudinal projected angle of incidence [°]
$\theta_t$	Transversal projected angle of incidence [°]
$\rho$	Density [kg/m <sup>3</sup> ]
$\rho_d$	Reflectance of a cover system for diffuse radiation incident from the bottom side [-]
$\sigma$	Stefan Boltzmann constant [W/m <sup>2</sup> K <sup>4</sup> ]
$\omega$	Angular frequency [1/s]

# 1 INTRODUCTION

Using solar thermal collectors is an environmentally friendly way of producing energy for space heating and/or domestic hot water since it causes no carbon dioxide emissions. The energy source is practically inexhaustible but the Swedish climate limits the use of solar collectors to late spring, summer and early fall. An auxiliary heating system is needed to cover the heating and domestic hot water load in the building all year round. The solar thermal systems are normally designed to barely cover the summer load in order not to over-size the system and thus make it as cost effective as possible. There is also a possibility of building systems with seasonal storage, but the storage space needs to be substantial to reduce the losses. This is only of interest for very large solar collector fields.

There are about 200 000 m<sup>2</sup> of installed solar collectors in Sweden. The major part of these installations consists of flat plate solar collectors. The market involves mainly small manufacturers and a large fraction of the production is manual. With a small market and mainly manual production the cost of solar energy is in most cases too high to compete with other energy supplies. There are generally speaking two ways to reduce the cost per produced kWh; either by increasing the efficiency at a moderate extra cost or to reduce the investment cost significantly without reducing the delivered energy output too much.

The primary aim of this work was to obtain more knowledge about solar thermal collectors and their components to be able to reduce the cost of energy produced with solar thermal collectors. The main part of the work was focused on studying a concentrating collector called the Maximum Reflector Collector, MaReCo, where the cost of solar energy heating is reduced by replacing part of the expensive absorber area with inexpensive reflector area and concentrate the incoming solar radiation.

The MaReCo has an asymmetrical design to fit the asymmetrical solar radiation distribution in Sweden. Different types of MaReCo have been developed for stand-alone, roof or wall mounting. The delivered energy output of the MaReCo is in general lower per aperture area than that of the flat plate collector. The purpose of the studies of the MaReCo concept was to optimise the design, increase the efficiency and further reduce the costs of the components in the collector to increase the benefit/cost ratio. Prototypes of MaReCo for stand-alone, roof and wall mounting were built and outdoor-tested at the Vattenfall Laboratory in Älvkarleby, Sweden. Hot-box measurements were performed to study heat losses for different collector component configurations in the stand alone MaReCo. To optimise the design of the geometry of the reflectors, detailed studies of the annual solar radiation distribution at different angles of incidence have been made to maximise the concentration ratio and still collect a high percentage of the available solar radiation.

Part of the work has concerned simulations of flat plate collectors. The flat plate solar thermal collector is by far the most common collector type on the market. Even though

the technology is well known there is still a lot that can be done to improve the efficiency of the flat plate collectors and to obtain more knowledge about the performance of flat plate collectors. For example not all roofs have the optimum tilt and azimuth. This initiated a study of how the delivered energy output from different flat plate solar collectors is affected by changes in tilt and azimuth. Another study presented in this work concerns the variation in delivered solar collector energy output with annual climate variations and how the delivered energy output varies with latitude in Sweden. The possibility of increasing the efficiency by optimising the material properties of the collector components was also investigated.

Two collector components, the reflector and the absorber have been studied in detail. A study of the scattering properties of two different reflector materials was made to investigate if a rough material can be used as a reflector in a solar collector. A spectrally selective Sunstrip absorber was investigated and one of the layers in the coating was analysed to optimise the absorbing properties.

This thesis involves studies from the material properties of the collector components to performance analyses of the whole collector. It is important to have knowledge about the components to be able to optimise the system. The work was carried out at the division of Solid State Physics, department of Materials Science, The Ångström Laboratory, Uppsala University. Traditionally this division studies the materials optics of solar collector components but through the involvement in the Energy Systems Programme some system studies have started. The Energy Systems Programme is a Swedish research school funded by the Foundation for Strategic Research, SSF, the Swedish Energy Agency, STEM, and Swedish industry.

## 2 THEORETICAL BACKGROUND AND EXPERIMENTAL METHODS

### 2.1 Collector analysis

The delivered energy output from the solar collector depends on the optical and thermal properties of the collector. This chapter contains a theoretical background of the parameters used to characterise the collector optically and thermally. Two methods to characterise the collector optically are presented. The first is to measure the optical properties of the absorber and the glazing and then calculate the zero loss efficiency and the incidence angle modifier. The second is through outdoor measurements where the optical and thermal properties of the collector are determined simultaneously by fitting to a collector model. Another method for thermal characterisation is also presented, indoor hot-box measurements. The components of the solar collector are presented.

#### 2.1.1 The solar collector

Two different collector types have been studied in this work, concentrating collectors and flat plate collectors. The major part has been focused on concentrating collectors, shown in a general sketch in Fig. 1.

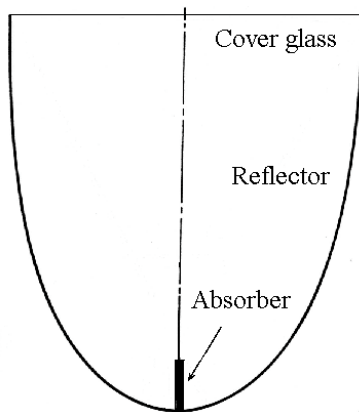


*Fig. 1 Sketch of a concentrating collector.*

The incoming light is reflected in the concentrating reflectors and then impinges on the absorber where it is transferred to the heat carrying medium. Because of the concentration the hot absorber area is reduced compared to that of the flat plate collector. The light is concentrated according to

$$C_i = \frac{A_{abs}}{A_c} \quad (1)$$

where  $A_{abs}$  is the absorber area and  $A_c$  is the aperture area.

In flat plate collectors, seen in Fig. 2, the absorbers are placed in an insulated collector box with a sealed glazing on top to reduce heat losses and to protect the absorber from rain and wind. An optional transparent insulation material (TIM) can be placed between the glass cover and the absorber to decrease heat losses by convection and radiation. In Fig. 2 a teflon film is shown. There are also more complex structures that can be used, for example honeycomb transparent insulation which consists of small plastic cells that are added together forming a honeycomb structure.

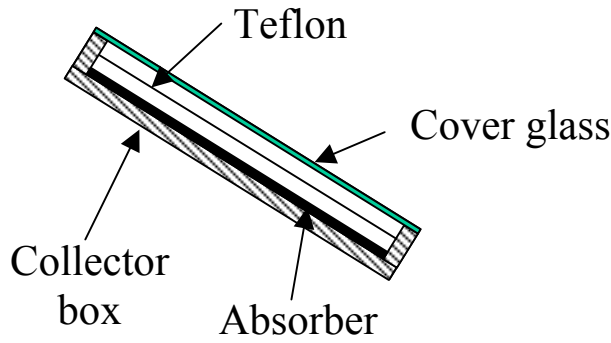


Fig. 2 Sketch of a flat plate solar collector.

The efficiency of a flat plate solar collector depends on its optical and thermal losses according to the basic energy balance equation (Duffie and Beckman 1991) in Eq (2).  $Q_u$  is the useful output,  $A_c$  is the collector area,  $S$  is the radiation absorbed by the collector per unit area of collector (incorporating the optical losses),  $U_L$  is the overall loss coefficient,  $T_{pm}$  is the mean plate temperature and  $T_a$  is the ambient temperature.

$$Q_u = A_c [S - U_L (T_{pm} - T_a)] \quad (2)$$

Optical losses originate from reflection of the solar radiation in the cover glass, the transparent insulation and the absorber surface. For the concentrating collector losses are added due to reflection losses and optical errors in the reflectors. Thermal losses are due to thermal conduction, convection and radiation. If the optical and thermal characteristics of the different components are known, collector parameters can be calculated and used in simulations to find the annual collector performance. The following sections describe the optical and thermal characterisation that is needed for this purpose.

### 2.1.2 Introduction to optics

The optical performance of a material depends on the wavelength of the incident light. The interaction of electromagnetic radiation with matter is described by the Maxwell equations (Wangsness 1986). In these equations electricity and magnetism are unified into electromagnetism. A propagating plane wave is described by

$$E = E_0 e^{\left[ i(\omega t - \frac{n}{c} \omega \vec{r} \cdot \vec{s}) - \frac{k}{c} \omega \vec{r} \cdot \vec{s} \right]} \quad (3)$$

where  $\vec{r}$  is the position vector and  $\vec{s}$  is the unit vector describing the direction of wave propagation in the chosen co-ordinate system. The optical refractive index,  $n$ , is the ratio of the speed of radiation (as light) in vacuum to that in the medium. The extinction coefficient,  $k$ , is a measure of the rate of extinction of transmitted light via absorption in the medium. The numerical values of  $n$  and  $k$  vary with material and wavelength. The quantities  $n$  and  $k$  define the complex refractive index and describe the optical behaviour of the electromagnetic radiation according to

$$N=n+ik \quad (4)$$

The Fresnel equations describe the reflection and transmission of light when passing from one medium to another. The ratio between the reflected and the incoming radiation, the amplitude reflectance, is for a bulk material described by

$$r_p = \frac{R_p}{A_p} = \frac{N_2 \cos \theta_1 - N_1 \cos \theta_2}{N_2 \cos \theta_1 + N_1 \cos \theta_2} \quad (5)$$

$$r_s = \frac{R_s}{A_s} = \frac{N_1 \cos \theta_1 - N_2 \cos \theta_2}{N_1 \cos \theta_1 + N_2 \cos \theta_2} \quad (6)$$

where  $p$  indicates p-polarised light and  $s$  indicates s-polarised light, index 1 refers to the medium before the interface and index 2 to the medium after the interface. Angles  $\theta_1$ , angle of incidence, and  $\theta_2$ , angle of refraction, are formulated in Snell's law

$$N_1 \sin \theta_1 = N_2 \sin \theta_2 \quad (7)$$

For incident unpolarised light the amounts of s- and p-polarised light are equal, and the reflectance is found as

$$R = \frac{|r_p|^2 + |r_s|^2}{2} \quad (8)$$

In solar energy materials a thin film is often applied on a substrate to obtain the desired optical properties. Such a case is sketched in Fig. 3. The arrows indicate the direction of light reflected from and transmitted through the film.

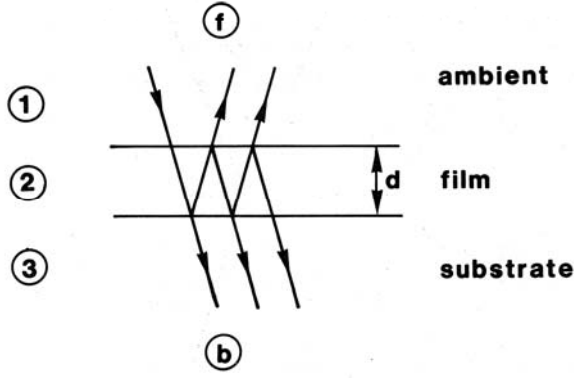


Fig. 3 Geometry used for describing the optics of a thin film on a substrate. *f*-front, *b*-back, *d*-film thickness. After Granqvist (1991).

Using the Fresnel's relations the amplitude reflectance for the film,  $r_2$ , is obtained from (Born and Wolf 1980).

$$r_{2s,p}^f = \frac{r_{s,p}^{12} + r_{s,p}^{23} e^{2i\delta}}{1 + r_{s,p}^{12} r_{s,p}^{23} e^{2i\delta}} \quad (9)$$

The measurable light intensity is denoted  $R$  and is given by

$$R_{2s,p}^{f,b} = |r_{2s,p}^{f,b}|^2 \quad (10)$$

This can be generalised into multiple layer films using matrix formalism further explained in for example Born and Wolf (1980). Each single layer is characterised by a matrix  $\bar{m}$

$$\bar{m} = \begin{pmatrix} m_{11} & m_{12} \\ m_{21} & m_{22} \end{pmatrix} \quad (11)$$

The elements in the matrix are

$$m_{11} = m_{22} = \cos\left[\frac{2\pi n(\lambda)d \cos \theta}{\lambda}\right] \quad (12)$$

$$m_{12} = -i \sin\left[\frac{2\pi n(\lambda)d \cos \theta}{\lambda}\right] / P \quad (13)$$

$$m_{21} = -iP \sin\left[\frac{2\pi n(\lambda)d \cos \theta}{\lambda}\right] \quad (14)$$

$$P = \sqrt{\frac{\varepsilon}{\mu}} \quad (\text{s-polarised}) \quad (15)$$

$$P = \sqrt{\frac{\mu}{\varepsilon}} \quad (\text{p-polarised}) \quad (16)$$

$N(\lambda)$  is the complex refractive index,  $d$  is the thickness of the single layer and  $\theta$  is the angle of incidence. The matrices of the single layers 1 to  $N$  are then multiplied using matrix multiplication to obtain the matrix  $\overline{M}$  for the stack of layers

$$\overline{M} = \overline{m}_1 \cdot \overline{m}_2 \dots \overline{m}_N \quad (17)$$

The reflectance of the coating with multiple layers is found from the matrix elements in  $\overline{M}$  according to

$$R = \left( \frac{(M_{11} + M_{12} P_{N+1})P_0 - (M_{21} + M_{22} P_{N+1})}{(M_{11} + M_{12} P_{N+1})P_0 + (M_{21} + M_{22} P_{N+1})} \right)^2 \quad (18)$$

$P_0$  and  $P_{N+1}$  denote the quantity  $P$  in Eq. (15) or (16) for the medium of incidence and the substrate respectively.

### 2.1.3 Introduction to thermal radiation

Thermal radiation is electromagnetic radiation described in Eq. 3 and travels at the speed of light. All bodies emit radiation according to their temperature, the blackbody is a perfect absorber and absorbs 100% of the incoming radiation and it is also a perfect emitter of thermal radiation. Planck's law (Nordling and Österman 1987) gives the wavelength distribution of the emitted radiation

$$I_b(\lambda, T) = \frac{2\pi c^2}{\lambda^5 [\exp(hC_0 / \lambda k_b T) - 1]} \quad (19)$$

The location of the maximum in the energy density is found through differentiating the Planck distribution and equating to zero. This relation is called Wien's displacement law (Duffie and Beckman 1991)

$$\lambda_{\max} T = 2897.8 \mu m K \quad (20)$$

For solar collector purposes the radiation distributions of the sun and the blackbody are important. Their maxima are separated according to Wien's displacement law. Before the solar radiation reaches the earth it is attenuated due to scattering and absorption in the atmosphere. Fig. 4 shows the solar radiation distribution with air mass 1.5 and a blackbody radiation distribution for a body of temperature 100°C.

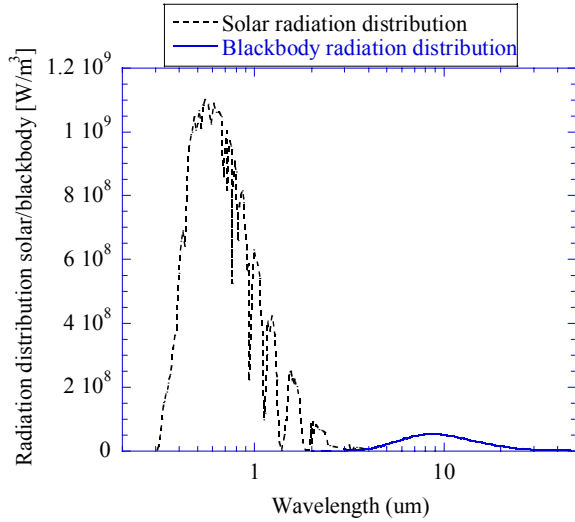


Fig. 4 Incident solar radiation distribution with air mass 1.5 according to the ISO standard 9845-1 (1992) (dotted) and blackbody radiation distribution for a temperature of 100°C.

If Planck's distribution is integrated over all wavelengths the total amount of energy emitted by the blackbody is obtained (Duffie and Beckman 1991)

$$I_b = \int_0^{\infty} I_b(\lambda, T) d\lambda = \sigma T^4 \quad (21)$$

where  $\sigma$  is the Stefan-Boltzmann constant equal to  $5.6697 \times 10^{-8} \text{ W/m}^2\text{K}^4$ .

## 2.1.4 Characterisation of solar collector components

### 2.1.4.1 Introduction

A thorough analysis of the optical properties of the components in the solar collector, such as reflector, absorber and glazing, is needed to understand the optical performance of the collector. Since the optical properties of the materials are wavelength dependent the optical characterisation has to be made in the appropriate wavelength range. For solar energy materials in low temperature solar collectors these are the solar spectral range 0.3 to 2.5  $\mu\text{m}$  and the infrared wavelength range up to about 50  $\mu\text{m}$ . The solar collector characterisation parameters can be obtained through various methods. The frequently used method in this work is based on spectral optical measurements.

Once the spectral reflectance and/or transmittance are known, the components can be characterised. The relation between the absorptance, transmittance and reflectance is

$$A(\lambda, \theta) + T_t(\lambda, \theta) + R(\lambda, \theta) = 1 \quad (22)$$

Using Kirchoffs law a relation between the light that is absorbed and emitted is found

$$A(\lambda, \theta) = E(\lambda, \theta) \quad (23)$$

### 2.1.4.2 Reflectors

A reflector material is characterised by the solar reflectance,  $R_{sol}$ .

$$R_{sol} = \frac{\int_{0.3}^{2.5} I_{sol}(\lambda)R(\lambda, \theta)d\lambda}{\int_{0.3}^{2.5} I_{sol}(\lambda)d\lambda} \quad (24)$$

$R(\lambda, \theta)$  is the spectral reflectance of the material at a certain incidence angle  $\theta$  and  $I_{sol}(\lambda)$  is the incident solar radiation distribution from Fig. 4.

The reflector quality is of great importance for the optical efficiency of the solar collecting device. High total reflectance in the solar wavelength range is important. Aluminium is often used in solar energy applications. If it is protected with an anodised layer it has a specular reflectance of approximately 80% and a total reflectance of 85% (Nostell et al 1997). If it is instead covered with a polyvinyl difluoride lacquer the corresponding values are around 75 and 83% (Nostell et al 1998). Silver has a significantly higher solar reflectance, but is also more expensive. Glass covered with a thin silver film has a specular reflectance of roughly 95%, depending on the glass (Paper VIII).

The surface roughness of the reflector determines how the reflected light is scattered. A measure of the surface roughness is the root mean square (rms) value,  $\delta_{rms}$

$$\delta_{rms} = \sqrt{\frac{1}{N} \sum_{i=1}^N z_i^2} \quad (25)$$

where  $N$  is the number of measurement points and  $z_i$  is the distance from the mean surface level. Light that is reflected by a surface as shown in Fig. 5 can be divided in three types. The specularly reflected light (a) is the light that is scattered within a small solid angle around an angle equal to the angle of incidence. To obtain specularly reflected light the surface must be smooth, i.e. the rms value is much smaller than the wavelength of the light incident on the surface. Isotropically scattered light is found for rough samples with no preferential structure leading to an equal scattering in all directions as in case (b). General scattering, (c), is found for surfaces with some preferential surface structure. A solar reflector generally exhibits anisotropic scattering with a specular component and a general component.

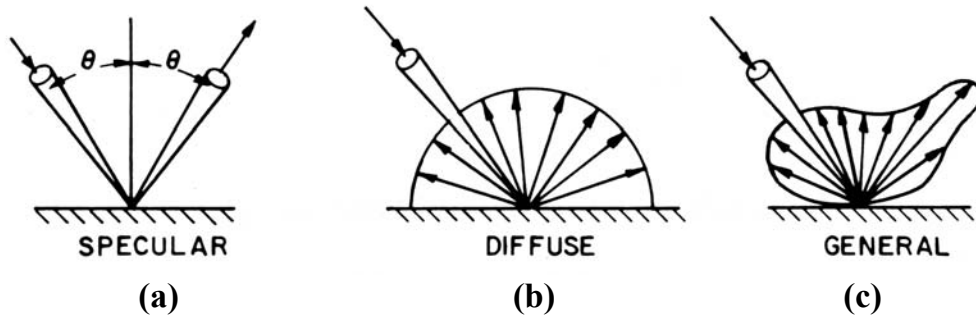


Fig. 5 Reflection from surfaces of different surface roughnesses from Duffie and Beckman (1991).

Most often high specular reflectance is preferable, but this is not always necessary. Low-concentrating devices, such as compound parabolic concentrators (CPC) are less sensitive to scattering of the incident radiation than high-concentrating devices such as parabolic troughs or dishes. Furthermore, if the non-specular radiation is scattered in linear corrugations with a particular geometry or unidirectional rolling grooves, this can be beneficial for certain concentrator geometries (Rönnelid and Karlsson 1998, 1999, Perers et. al 1994). Since rolled aluminium is cheap compared to other reflector materials, it can be a cost-effective and suitable material for certain solar energy applications. It is therefore of interest to characterise reflectance and light scattering from rolled aluminium of different surface roughness in order to evaluate their feasibility as reflector materials. If a rough material with rolling grooves is studied the scattering from the material shows a very characteristic pattern, depending mainly on the orientation of the rolling grooves. A very large part of the reflected radiation is scattered as in one-dimensional reflection gratings.

Angle resolved scattering, ARS, were performed to obtain more information about the optical scattering of the reflectors. A method to characterise and evaluate the scattering properties was developed in Paper IX, based on adding ARS-data together in different regions according to:

Specular reflectance, SR- The radiation reflected between  $|\phi| < 3^\circ$  and  $|\theta| < 3^\circ$

Low -Angle Scattered Light in the Scatterband, LAS-B- The radiation reflected within the angular range  $3^\circ < |\phi| < 9^\circ$  and  $3^\circ < |\theta| < 9^\circ$  within the scatterband

Low-Angle Scattered light, LAS- The radiation reflected between  $|\phi| < 9^\circ$  and  $|\theta| < 9^\circ$  excluding the radiation found in SR and LAS-B

High-Angle Scattered Light in the Scatterband, HAS-B- The radiation reflected between  $|\phi| > 9^\circ$  and  $|\theta| > 9^\circ$  within the scatterband

High-Angle Scattered Light, HAS- The radiation reflected between  $|\phi| > 9^\circ$  and  $|\theta| > 9^\circ$  that is not included in HAS-B

The angle  $\phi$  refers to the angular deviation from the specular direction in the direction perpendicular to the plane created by the surface normal and the incoming beam (azimuthal angle).  $\theta$  is the deviation from the specular spot in the direction parallel to the plane created by the surface normal and the incoming beam. A feasible reflector

should have a large part of the reflected radiation within the SR region, especially if the material is used as an internal reflector, like for example in a compound parabolic concentrator.

### 2.1.4.3 Absorbers

To investigate how much of the radiation that will be absorbed and thermally re-emitted, the spectral reflectance can be recorded in the solar wavelength interval, approximately 0.3 to 2.5  $\mu\text{m}$  and in the infrared interval, approximately 2.5 to 20  $\mu\text{m}$ . In Fig. 6 the reflectance curve for a spectrally selective absorber is shown together with the spectral distribution of solar radiation (dotted) and the spectral distribution of blackbody radiation for a surface with  $T=100^\circ\text{C}$  from Fig. 4.

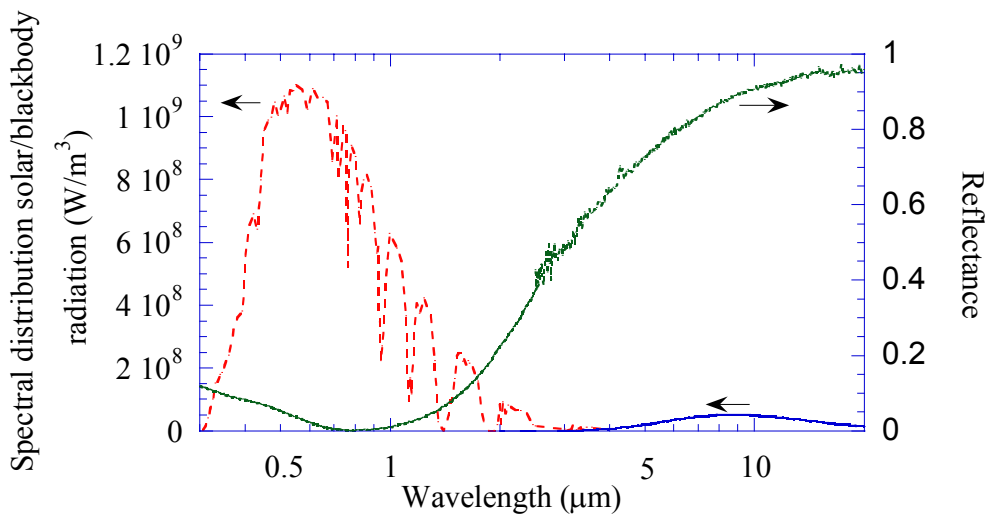


Fig. 6 Incident solar radiation distribution with air mass 1.5 according to the ISO standard 9845-1 (1992) (dotted), blackbody radiation distribution for absorber plate temperature  $100^\circ\text{C}$  and measured reflectance for a sputter deposited spectrally selective solar absorber.

In order to obtain the solar absorptance and thermal emittance, the measured spectral reflectance is weighted against the solar spectrum and a thermal spectrum, respectively. The spectral distribution of the solar radiation depends on which air mass is chosen. For an opaque object Eq. (22) and (23) leads to the relation

$$A(\lambda, \theta) = E(\lambda, \theta) = 1 - R(\lambda, \theta) \quad (26)$$

The solar absorptance is found through

$$\alpha_{sol} = \frac{\int_{0.3}^{2.5} I_{sol}(\lambda)(1 - R(\lambda, \theta))d\lambda}{\int_{0.3}^{2.5} I_{sol}(\lambda)d\lambda} \quad (27)$$

where  $R(\lambda, \theta)$  is the reflectance distribution.

The hemispherical thermal emittance of the absorber at temperature T is found through

$$\varepsilon_{therm} = \frac{\int_{2.5}^{20} [1 - R(\lambda, \theta)] I_b(\lambda, T) d\lambda}{\int_{2.5}^{20} I_b(\lambda, T) d\lambda} \quad (28)$$

where  $I_b(\lambda, T)$  is the spectral distribution of blackbody radiation at temperature T from Eq (19).

Typical values of  $\alpha_{sol}$  and  $\varepsilon_{therm}$  for a spectrally selective absorber are 0.93-0.96 and 0.05-0.25 respectively. The spectrally selective absorber shown in Fig. 6 is characterised by  $\alpha_{sol}=0.95$  and  $\varepsilon_{therm}=0.10$ . Further reading on spectrally selective absorbers is found in Wäckelgård et al (2001) or Granqvist (1991). If the absorber is non-selective, as ordinary black paint,  $\alpha_{sol}$  and  $\varepsilon_{therm}$  have about the same value, around 0.95. An ideal spectrally selective absorber would have  $R(\lambda, \theta)$  equal to zero throughout the whole solar spectrum and equal to unity in the thermal range, but this is not possible with the materials known today.

#### 2.1.4.4 Glazing

The solar transmittance is found by integrating the transmittance of the material with the solar spectrum at each wavelength and incidence angle according to (Duffie and Beckman 1991)

$$T_{sol} = \frac{\int_{0.3}^{2.5} I_{sol}(\lambda) T_t(\lambda, \theta) d\lambda}{\int_{0.3}^{2.5} I_{sol}(\lambda) d\lambda} \quad (29)$$

where  $T_t(\lambda, \theta)$  is the transmittance distribution at angle  $\theta$ .

Typical values of solar transmittance are for ordinary float glass 83-85% and for low iron glass 90% (Nostell et al 1999). Low iron glass is the most frequently used glass for solar collector covers, and the transmittance is fairly constant over the solar spectrum. Ordinary float glass has a more wavelength dependent transmission. Teflon film used in solar collectors has a solar transmittance of 96% (Rönnelid and Karlsson 1996). Honeycomb (HC) transparent insulation material has a  $T_{sol}$  that depends on the material and the geometry. Poly-carbonate HC with a cell size 3.5x3.5 mm of thickness 50 mm and 100 mm and have a diffuse  $T_{sol}$  of 81% and 75% respectively.

### 2.1.5 Instruments for optical characterisation

The spectral measurements were in general obtained with a spectrophotometer equipped with an integrating sphere in the 0.3-2.5  $\mu\text{m}$  region and an FTIR (Fourier Transform Infra Red) spectrophotometer in the 2.5-20  $\mu\text{m}$  region. One example of such a measurement is found in Fig. 6 where the reflectance for a spectrally selective absorber is shown. The measured spectral reflectance was then used to determine the integrated values  $R_{\text{sol}}$ ,  $\alpha_{\text{sol}}$ ,  $\epsilon_{\text{therm}}$  and  $T_{\text{sol}}$  in a numerical integration routine.

Absolute measurements of spectral specular reflectance and transmittance at different angles of incidence were performed in a non-standard spectrophotometer equipped with an integrating sphere as detector. The sample is placed in the centre of a horizontal ring, in a holder, which can rotate around its vertical axis. The detector can be swept around the ring then allowing for measuring the specular reflectance and transmittance at different angles of incidence. Description in detail of this measuring system is published in Roos (1997).

Profilometry was used to investigate the surface roughness of reflector materials. In this case white light optical microscopy was used, a WYKO NT-2000 interference fringe microscope with a Mirau interferometer. This was used to obtain the surface root mean square height and slope and the power spectral density function.

Angle resolved scattering, ARS, was measured with a set up shown in Fig. 7. A red He-Ne laser (633 nm) was used as a light source. The sample could be tilted to vary the angle of incidence on the sample. The detector was placed on a device that could move over the sphere in angles  $\theta$  and  $\phi$  (defined in Fig. 7) allowing it to measure the intensity in three dimensions. The distance between the measurement points was determined by the intensity of the signal; shorter steps were taken when the signal level was high.

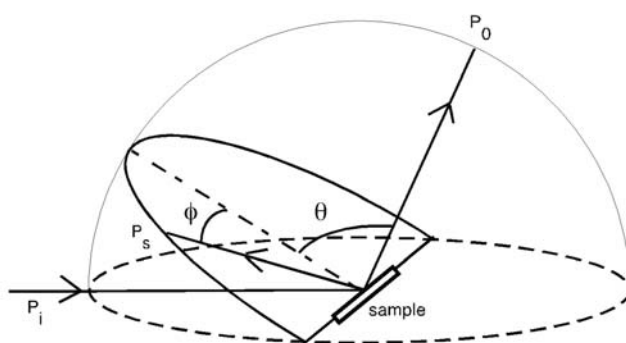


Fig. 7 Schematic drawing of the ARS measurement equipment.  $P_i$ , incident beam;  $P_s$ , scattered intensity;  $P_0$ , the specular component. Angles  $\theta$  and  $\phi$  are the in-and out-of-plane scattering angles, respectively.

Spectral measurements were also made with total integrated scattering, TIS, in the region 0.37-0.97  $\mu\text{m}$  (Rönnow and Veszelei 1994). With TIS a focusing half-sphere with the detector placed in the focal point is used. Due to the focusing properties very

low intensities can be detected. To validate the ARS-measurements screens were used that covered parts of the half-sphere in fixed angular intervals (Rönnow 1997).

## 2.1.6 Collector heat losses

### 2.1.6.1 Introduction

In a solar collector, energy is lost through radiation, convection and conduction. Losses through thermal radiation introduced in section 2.1.3 are significant in the case of a solar collector since the total energy transfer is low and thereby the radiation losses are a large part of the total losses. This chapter reviews selected parts of the heat transfer that is important in a solar collector starting with radiation heat transfer and then proceeding with a short section on convection and conduction. These losses are usually added together in one quantity, the overall loss coefficient  $U_L$  of the collector, and includes the top, bottom and edge losses.

The heat losses of a solar collector can be experimentally determined in a number of ways, for example through hot-box measurements or outdoor/solar simulator collector tests. They can also be determined through theoretical calculations. Two of these methods have been used in the work presented in this thesis; hot-box measurements and outdoor collector tests.

### 2.1.6.2 Radiation heat transfer

When  $N$  surfaces are facing each other a radiation exchange takes place. The amount of energy that surface  $i$  exchanges pair wise with the  $N-1$  other surfaces,  $Q_i$ , depends on the emittance of the surfaces,  $\varepsilon_i$  &  $\varepsilon_j$ , exposed area of surface  $i$ ,  $A_i$ , total exchange factor,  $\hat{F}_{ij}$ , and temperature difference between the surfaces according to Eq. (30) (Duffie and Beckman 1991). The exchange factor depends on how the surfaces emit radiation, if there is a specular component or if the radiation is diffuse and the view factor. If the reflected radiation from the surface lacks a specular component the exchange factor is reduced to the view factor. The assumptions that are made are that the surface is grey (radiation properties are independent of wavelength), diffuse or specular-diffuse, has a uniform temperature difference and that the incident energy over the surface is uniform.

$$Q_i = \sum_{j=1}^N \varepsilon_i \varepsilon_j A_i \hat{F}_{ij} \sigma (T_j^4 - T_i^4) \quad (30)$$

A large part of the heat transfer problems in solar energy applications involve radiation between two surfaces. Eq. (30) is then simplified to

$$Q_1 = -Q_2 = \frac{\sigma(T_2^4 - T_1^4)}{\frac{1 - \varepsilon_1}{\varepsilon_1 A_1} + \frac{1}{A_1 F_{12}} + \frac{1 - \varepsilon_2}{\varepsilon_2 A_2}} \quad (31)$$

Two special cases of this relation are useful:

1. Two infinite parallel surfaces, i.e. a flat plate collector, where the areas are equal and the view factor is unity:

$$Q = A\sigma \frac{(T_2^4 - T_1^4)}{\frac{1}{\varepsilon_1} + \frac{1}{\varepsilon_2} - 1} \quad (32)$$

2. The radiation exchange between the sky and a collector, the sky is considered a blackbody radiator with sky temperature  $T_s$ . In this case the collector is considered small compared to the surrounding sky ( $A_1/A_2 \rightarrow 0$ ) and the view factor is unity. The relation is simplified to

$$Q = \varepsilon_1 A_1 \sigma (T_2^4 - T_s^4) \quad (33)$$

To simplify to linear relations in Eq. (31) the radiation heat transfer coefficient,  $h_r$ , is introduced according to

$$Q = A_1 h_r (T_2 - T_1) \quad (34)$$

where

$$h_r = \frac{\sigma(T_2^2 - T_1^2)(T_2 + T_1)}{\frac{1 - \varepsilon_1}{\varepsilon_1} + \frac{1}{F_{12}} + \frac{(1 - \varepsilon_2)A_1}{\varepsilon_2 A_2}} \quad (35)$$

### 2.1.6.3 Convection heat transfer

Heat is also transferred through natural convection in the solar collector. The air that is closest to the hot surface is heated and the density is lowered. This causes the hot air to rise and cold air to fall and a flow of air is created. The rate of heat transfer is described with the Nusselt-, Rayleigh- and Prandtl number. These quantities are dimensionless and depend on material properties, temperature difference between the surfaces and spacing. They are further described, for example, in Duffie and Beckman (1991). The natural convection can be suppressed through transparent insulation in the spacing, for example a single teflon sheet or a honeycomb structure.

### 2.1.6.4 Conduction heat transfer

When two media are in contact heat is transported from the hot medium to the cold by transferring kinetic energy from one molecule/atom to an adjacent molecule/atom. The amount of energy that is transferred is dependent on temperature difference, contact area and heat conductivity in the participating materials. Conduction can occur for example through the insulation in the collector box.

### 2.1.6.5 Collector overall loss coefficient

The collector overall loss coefficient  $U_L$  is used to characterise the heat losses in Eq. (2).  $U_L$  is the sum of the heat losses from top, back and edges:

$$U_L = U_t + U_b + U_e \quad (36)$$

The major part of the heat losses escapes through the top of the collector. According to Morrison (2001) the back and edge losses are of the order of 10% and 5% respectively of the top losses.

If the sky temperature is approximated with the ambient temperature; the top loss coefficient is found as (Morrison 2001):

$$U_t = \frac{1}{\frac{1}{h_1 + h_2} + \frac{1}{h_3 + h_4'}} \quad (37)$$

where:

- $h_1$  Internal convection coefficient, 3-5 W/m<sup>2</sup>K
- $h_2$  Plate to cover radiation coefficient, 6-8 W/m<sup>2</sup>K for  $\epsilon_p=1.0$  and 0.6-0.8 W/m<sup>2</sup>K for  $\epsilon_p=0.1$  (Calculated with Eq. 35)
- $h_3$  External convection coefficient, 5.8 W/m<sup>2</sup>K for V=1 m/s and 8.8 for V=2 m/s
- $h_4$  External radiation coefficient for clear sky conditions, 5-6 W/m<sup>2</sup>K

The use of a spectrally selective absorber thus reduces the heat losses significantly compared to using a black painted absorber since  $h_2$  is decreased with a factor of 10. The heat losses can also be reduced by including some kind of convection suppression, for example teflon film or honeycomb transparent insulation which reduces the internal convection coefficient and the radiation losses.

The back losses depend on the insulation thickness,  $L$ , and conductivity,  $k_c$ , according to (Duffie and Beckman 1991)

$$U_b = \frac{k_c}{L} \quad (38)$$

The edge losses depend on the edge loss coefficient-area product and the collector area (Duffie and Beckman 1991):

$$U_e = \frac{(UA)_{edge}}{A_c} \quad (39)$$

When characterising a collector experimentally the temperature dependence of the collector overall loss coefficient can be assumed to be linear (Duffie and Beckman 1991)

$$U_L = U_1 + U_2(T_{pm} - T_a) \quad (40)$$

Where  $U_1$  is the first order heat loss coefficient and  $U_2$  the second order heat loss coefficient that determines the temperature dependence in the overall loss coefficient.

#### 2.1.6.6 Heat loss collector characterisation methods

Two methods of characterising heat losses have been used in this work, the hot-box method and the outdoor test method.

The major draw back with the hot-box method is that the obtained U-value is not directly applicable for outdoor conditions but rather a laboratory U-value, since wind and sky effects are not taken into account. Another difference is that in the hot-box measurement only the absorber plate is heated while in a collector placed outdoors the whole collector is heated. This difference is especially important for a concentrating collector where the absorber area is smaller than the aperture area. Corrections are needed to compensate for these differences before the values are used to estimate an annual delivered energy output with simulations. The advantages are that no real prototype is needed, only a simplified collector construction can be used. It is also possible to study the materials in the collector one by one in a standardised equipment that facilitates comparison measurements.

The thermal parameters obtained with the outdoor test method are directly applicable in collector simulations to get an estimate of the annual performance of the collector and not only laboratory U-values. Another advantage with this method is that the thermal and optical performance are obtained simultaneously. With this method a collector prototype needs to be built and it is harder to evaluate the materials in the collector separately.

#### *The hot-box method*

The regular absorber is replaced by an electrically heated absorber plate simulating the warm absorber. This method was used to characterise the heat losses in a stand alone MaReCo in Paper II.

To measure the U-value with the hot box method thermocouples are attached to measure the temperature of the heated absorber plate,  $T_{pm}$ , and the ambient,  $T_a$ . The laboratory collector overall loss coefficient is then calculated through:

$$U_L^{lab} = \frac{V_e I_e}{A_c (T_{pm} - T_a)} \quad (41)$$

where  $A_c$  is the aperture area,  $V_e$  is the applied voltage and  $I_e$  is the current. Steady state is in general reached after several hours, depending on the thermal inertia of the

collector. The hot-box method can be used for flat plate and concentrating collectors and also to test the thermal properties of materials like for example transparent insulation. In the latter case the electrically heated absorber is placed in a well insulated box and the material to be investigated is placed covering the top of the box.

If the applied electric power is varied a series of U-values at different temperature differences between the absorber and the ambient is obtained as seen in Fig. 8. The linear relation was suggested in Eq. (40), and a linear fit is therefore indicated by the solid line in Fig. 8.

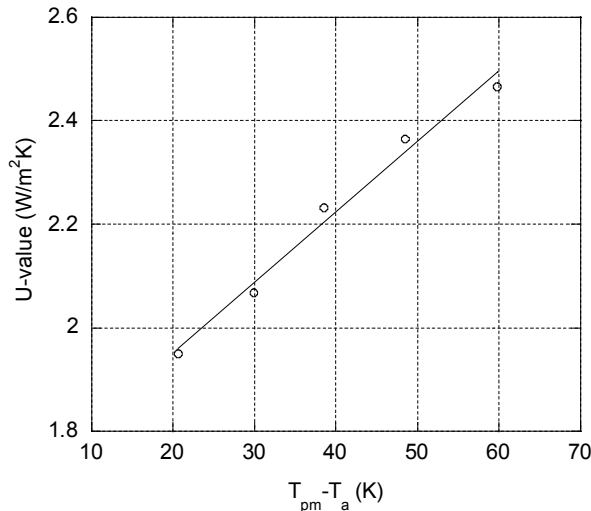


Fig. 8 U-value as a function of temperature difference between absorber and ambient for a stand-alone MaReCo with spectrally selective, vertical absorber and open ventilation channels. The solid line indicates a least square fit of the measurements.

The hot-box technique can also be used to study the temperature distribution within the collector. It is especially important if temperature sensitive materials such as polycarbonate transparent insulation is used in the collector. In this case thermocouples are placed at the points of interest in the collector box and then the applied power is varied.

#### *Outdoor collector efficiency tests*

The test site for outdoor measurements described in this thesis is situated at the Älvkarleby Laboratory and it has the capacity to evaluate up to 15 collectors at the same time. It has two main systems, one in which the inlet temperature at each collector can be controlled in order to get a variety of operating conditions and one system where all collectors are connected in series with a common flow, facilitating comparison measurements. In the common flow system, which was used in the evaluation in Paper I, the water is cooled after each collector to get the same inlet temperature for all collectors. With this arrangement, where all collectors have the same water flow, possible uncertainties in flow measurements have no effect on the comparison measurements. The collector inlet and outlet temperatures were registered together with the flow of water/glycol. The ambient temperature and solar radiation (global and diffuse) measured both on a horizontal surface and in the collector plane were recorded. The radiation was also measured with a sun tracking pyranometer and a

tracking pyrheliometer. The diffuse radiation was measured by using a shadow ring on the pyranometer. All data were sampled with a Campbell Scientific data logger every 10:th second and the sampled values were stored as 10 minutes mean values.

Flow, temperatures and irradiation were measured during a number of days with various combinations of irradiation and collector temperatures. From these data, the energy output,  $q_u$ , was calculated according to

$$q_u = \rho V c_p (T_{out} - T_{in}) / A_c \quad (42)$$

where  $\rho$  represents density,  $V$  volume,  $c_p$  heat capacity,  $T_{out}$  temperature out of the collector,  $T_{in}$  temperature into the collector and  $A_c$  aperture area.

The incidence angle for beam radiation in the collector plane and the measured- and the estimated output from the prototypes were calculated from the measured data. The collector parameters in Eq (43) were then determined with the method of dynamic testing using Multiple Linear Regression, MLR, on measured data. With the dynamical testing method collectors can be evaluated not only during perfectly clear days but also during partly cloudy days. The method is further described in Perers (1993 and 1997) and Perers and Walletun (1991). The dynamic testing model has been compared to other test methods and is considered theoretically complete taking almost all effects into account (Nayak and Amer 2000). The parameters obtained with the dynamic testing model are: beam zero loss efficiency,  $F'(\tau\alpha)_b$ , diffuse zero loss efficiency,  $F'(\tau\alpha)_d$ , first order heat loss coefficient,  $F'U_{L1}$ , second order heat loss coefficients,  $F'U_{L2}$ , collector thermal capacitance,  $(mC)_e$ , incidence angle modifier,  $K_{\tau\alpha}$ . The incidence angle modifier can be expressed either as the incidence angle modifier coefficient,  $b_0$ , or by an incidence angle dependence matrix. These parameters are further described in section 2.1.7.

In order to verify the parameters determined by the dynamic testing model different diagrams are drawn. In a daily diagram the measured and the modelled output are compared during a whole day. An example of this is found in Fig. 9, where it can be seen that the agreement between the model and the measured data is very good. The diagram also shows the daily irradiation. The energy output obtained with the dynamic testing method follows the measured output even if there are sudden changes in irradiation, e.g. rapidly passing clouds as seen in Fig. 9. In a model/measurement-diagram, the simulated output is plotted versus the measured output. This is shown in Fig. 10. Ideally the dots should form a straight line  $y=x$ . The parameters obtained from the dynamic testing-model are then fed into a simulation program to get an estimate of the annually delivered energy output.

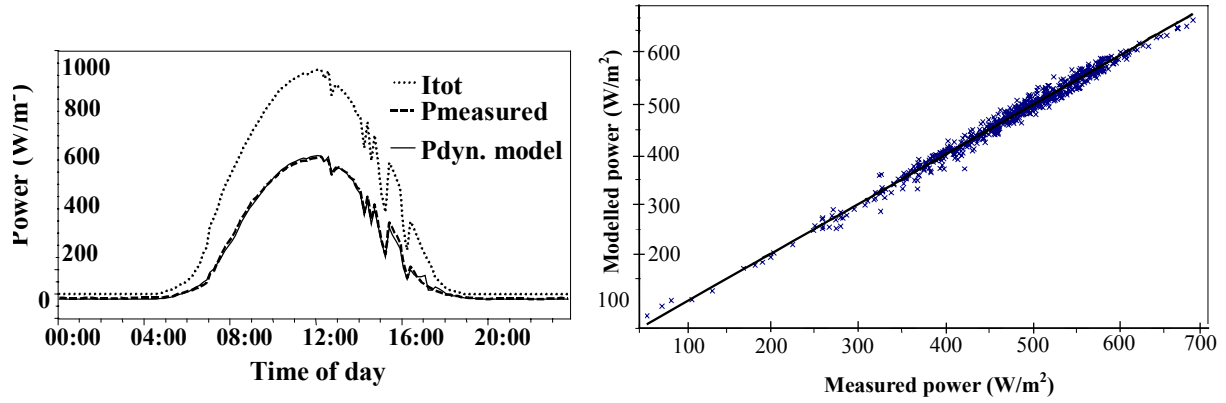


Fig. 9 Daily diagram from August 28<sup>th</sup> 2000 showing global radiation, modelled power from the dynamical testing model and MaReCo. The solid line indicates a linear fit measured power in  $W/m^2$  for the concentrating collector.

### 2.1.7 Characterisation of the collector

The useful delivered energy output of a collector working under steady-state conditions is given by (Perers 1995)

$$q_u = F'(\tau\alpha)_b K_{\tau\alpha b}(\theta) G_b + F'(\tau\alpha)_d K_{\tau\alpha d}(\theta) G_d - F'U_{L1}\Delta T - F'U_{L2}(\Delta T)^2 - (mC)_e dT_f/dt \quad (43)$$

The collector efficiency factor,  $F'$ , accounts for the temperature variation over the absorber, the fins have a higher temperature than that of the heat carrying medium. The value of  $F'$  depends on the ability of the absorber to transfer the energy that is absorbed in the fin to the riser tube.

The  $(\tau\alpha)$ -product takes into account that some of the radiation that is reflected from the absorber is then in turn reflected in the glazing back to the absorber (Duffie and Beckman 1991)

$$(\tau\alpha) = \frac{\tau_{sol} \alpha_{sol}}{1 - (1 - \alpha) \rho_d} \quad (44)$$

where  $T_{sol}$  is the solar transmittance of the glazing from Eq. (29),  $\alpha_{sol}$  is the solar absorptance of the absorber from Eq. (27) and  $\rho_d$  is the reflectance of a cover system for diffuse radiation incident from the bottom side.

The product of the fin efficiency and the  $(\tau\alpha)$ -product is also denoted the zero-loss efficiency,  $\eta_0$ , and describes the efficiency of the collector when it is operating at ambient temperature when no thermal losses are obtained.

The angular dependence of the solar collector is characterised by the incidence angle modifier,  $K_{\tau\alpha}$  (Duffie and Beckman 1991)

$$K_{\tau\alpha} = \frac{(\tau\alpha)}{(\tau\alpha)_n} \quad (45)$$

The index  $n$  indicates normal incidence. A general empirical expression that is widely used for flat plate collectors incorporating the incidence angle modifier coefficient,  $b_0$  is (Duffie and Beckman 1991)

$$K_{\tau\alpha} = 1 + b_0 \left( \frac{1}{\cos\theta} - 1 \right) \quad (46)$$

The angular dependence of the beam and the diffuse radiation are handled separately. For the beam radiation the angle of incidence of the beam radiation is used for  $\theta$  in Eq. (46) and for the diffuse radiation an effective angle of incidence obtained for example from Duffie and Beckman (1991) is used.

The loss coefficients  $U_{L1}$  and  $U_{L2}$  are found by dividing  $U_1$  and  $U_2$  from Eq. (40) by the fin efficiency  $F'$ . The term  $(mC)_e$  describes the thermal inertia of the collector. Part of the absorbed energy is lost to heating the collector in the morning when the collector starts to operate and then partly regained in the afternoon before the collector is turned off.  $(mC)_e$  also describes how the collector reacts with rapid changes in solar radiation and wind.

## 2.2 Collector simulations

### 2.2.1 Introduction

Computer based model simulations of solar collectors are frequently used methods of deriving the delivered energy output from the collector. Alterations in the collector are easily made and evaluated and compared to other simulated results or measurements. The number of solar collector models is of the same order as the number of people who do collector simulations. All these programs have their own specialities, but can roughly be divided into five groups, starting with the most simple “program”, the nomogram and ending with very complex programs studying very specific parts of the collector. A short review is given below.

1. Nomograms where the output can be determined by following some simple steps. These nomograms are based on either calculations or measurements. As an example the solar heating nomogram made by Bengt Perers, Vattenfall Utveckling AB can be mentioned. This was compiled within the CEC Thermie B Project: Solar Heating in Northern and Central Europe. In only a couple of minutes it is possible to get the estimated delivered energy output.

2. Correlation based programs with long time steps, often daily time steps. They are often built on a large number of detailed sub-simulations made with another program. Running time typically about 1 minute. An example of this kind of program is the F-Chart.
3. Programs with hourly time steps in climate data and components based on physics, taking first order effects into account. MINSUN is one example of this kind of program, and has an executing time of less than a minute. TRNSYS is probably a better known example, with a running time of less than 15 minutes. TRNSYS is perhaps the most frequently used simulation program used today (2002). The largest advantage with TRNSYS is that it is flexible, since it is module based. Different modules can be put together to simulate all sorts of complex systems.
4. Very detailed models on a component level. Time steps are normally less than one hour and they are typically designed to investigate a very particular effect for a certain collector type. These are not commercial programs, but often written by a PhD-student for very specific cases.
5. Programs based on finite element methods designed to investigate problems on the level of basic physics, for example convection. Very computer power demanding and no commercial programs available.

For the type of simulations used in this thesis, programs from group 3 are the most suitable. The MINSUN program was chosen because it is very easy to learn and has a rather advanced collector model that is well validated with experimental data. It can also be used to simulate a whole building, but that option is not used here.

### 2.2.2 The MINSUN program

The MINSUN simulation program was originally developed to speed up simulations of large solar energy systems with seasonal storage. The program consists of two parts, the solar collector array model and the system model including storage, district-heating net, heat loads, and domestic hot water loads (Chant, 1985). Since the first MINSUN version, the collector array model has been further developed with additional correction terms and functions using experience from solar collector testing (Perers 1993a,b).

In this thesis only the collector array part was used. The collector array part of the MINSUN simulation program was chosen here because no knowledge about the system outside the collector array is needed, for example heat loads, tank sizes etc. Instead of detailed system information the program uses a fixed average operating (heat carrier fluid) temperature,  $([T_{in}+T_{out}]/2)$ . Five different average operating temperatures can be simulated at once

The well-defined operating conditions make a comparison between different collectors more straight forward, since no system effects are included. If the operating

temperature is varying within relatively small limits, this approximation is valid even for a collector in a system.

In the solar collector model hourly steps are used in the calculations. The useful energy output,  $q_u$ , of the collector is calculated with the MINSUN program by the energy balance in Eq (43).

The collector parameters zero-loss efficiency (beam and diffuse)  $\eta_{0b}$  and  $\eta_{0d}$ , loss coefficients  $U_{L1}$  and  $U_{L2}$ ,  $(mC)_e$  and  $b_0$  together with the collector tilt and azimuth are fed into the program together with hourly climate data with beam and global radiation and ambient temperature. The output from the program is presented in three different files. A log-file with a presentation of the collector parameters and then a summary with monthly/annual mean values of beam and total radiation, ambient temperature, collector energy output and operating time at different operating temperatures is the most frequently used. The other two files contain hourly values of the above mentioned parameters together with various information on for example solar height, azimuth etc.

The delivered collector output obtained with the MINSUN program can then be used to analyse for example the collector dependency on tilt and azimuth for various collectors (Paper VII), the impact of material properties on the collector energy output (Paper VIII), the influence of annual climate variations on collector energy output (Paper VI) or the expected annual energy output for a collector in an outdoor test (Paper I).

## 2.3 Optical characteristics of nonimaging concentrating collectors

### 2.3.1 Introduction

If part of the expensive absorber area is replaced by cheap reflectors the cost of the energy produced with solar collectors is reduced. The thermal losses are in general lowered if the light is concentrated since a smaller area of hot absorber is required to produce a certain amount of heat. The reduced losses also make it possible to reach higher absorber temperatures than those obtained with flat plate solar collectors.

There are a number of ways to obtain the concentration of the light; for example with reflectors and lenses. Concentrators are treated in two main groups, imaging and nonimaging. In a nonimaging collector all radiation that impinges on the aperture, beam and diffuse, that is within a certain angular interval is reflected onto the receiver. These collectors function seasonally with minimum or no requirements of tracking. The concentrators studied in this work are all nonimaging.

The most common nonimaging concentrator is the compound parabolic concentrator, the CPC, with the original concept developed by Hinterberger and Winston (1966). Since then the concept has been further developed by for example Rabl (1976) and

Mills and Giutronich (1978). The CPC-collector is described in more detail in for example Welford and Winston (1989), Duffie and Beckman (1991) or Winston (2001). The basic CPC concept with a cross section of a symmetrical nontruncated CPC is shown in Fig. 11 (Duffie and Beckman 1991). The collectors are mainly used as linear or trough-like concentrators.

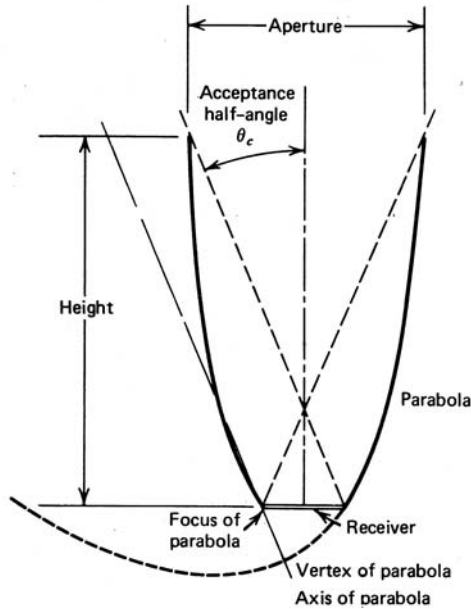


Fig. 11 Cross section of a symmetrical nontruncated CPC (from Duffie and Beckman 1991).

The acceptance interval defines the angular interval within which all radiation is transferred from the aperture to the receiver, and the acceptance half-angle shown in Fig. 11 is half of the acceptance interval. For a full CPC, the collector height defined in Fig. 11 tends to be long. The height of the CPC is often truncated by cutting the reflectors to a shorter length. This saves reflector area with a small reduction in performance.

The area concentration factor for a concentrating collector is defined as the ratio of the aperture area to the receiver area according to Eq. (1). For an ideal two-dimensional non-truncated CPC this is given by (Duffie and Beckman 1991)

$$C_i = \frac{1}{\sin \theta_c} \quad (47)$$

A number of concentrating collector types are denoted CPC-collectors even though they have other reflector geometries than the parabolic.

### 2.3.2 Description of the Maximum Reflector Collector, MaReCo

The MaReCo is an asymmetrical truncated trough-like CPC collector designed for high latitudes. It is non-tracking, has a bi-facial absorber and can be designed for various system conditions, for example stand alone mounting on ground or roof integrated. The aim is to design a low cost solar collector without reducing the performance too much compared to a flat plate collector. Expensive absorber area is replaced by cheap reflector area.

Several other studies of asymmetric concentrating collectors have been reported by, for example, Tripanagnostopoulos et al. (1999 and 2000), Norton et al. (1991), Welford and Winston (1989), Mills and Giutronich (1978) and Rabl (1976). A study of ultra flat concentrators suitable for building integration has been made by Chaves and Collares-Pereira (2000). Three large stand-alone ground mounted MaReCo systems have been constructed and are described in Karlsson and Wilson (1999).

A CPC trough according to Fig. 12 is designed with two parabolas with their optical axes given by the lower and upper acceptance angles. The reflector consists of three parts. Part C is a lower side parabola extended between points 1 and 4 in Fig. 12. This parabola has its optical axis directed towards the upper acceptance angle and focus on the top of the absorber. Part B is a circular part between points 1 and 2. This circular part transfers the light onto the absorber. It replaces a second absorber fin that otherwise would have been needed between focus and point 2 (indicated by a dotted absorber between points 2 and 5 in Fig. 12). The lower tip of the absorber can be placed anywhere along the circle sector between points 1 and 2. Part A is a parabolic upper reflector between the points 2 and 3 in Fig. 12. This parabola has its optical axis along the lower acceptance angle and its focus at point 5.

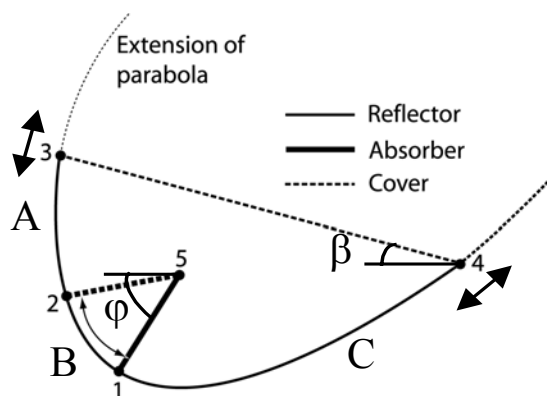


*Fig. 12 Sketch of the basic MaReCo design. Part A is the upper parabolic reflector extended from points 2-3, Part B is the connecting circular reflector extended from points 1-2, Part C is the lower parabolic reflector extended from points 1-4. The cover glass is found between points 3 and 4. The position of the cover glass varies along the extended parabola depending on the truncation.  $\beta$  is the aperture tilt and  $\phi$  is the absorber inclination angle.*

The position of the cover glass (i.e. the position of points 3 and 4 along the extended parabolas in Fig. 12) is determined by varying the position of the reflector along the extended parabolas to find the position where maximum annual irradiation onto the

aperture is obtained. When designing the collector prototypes this was made by sliding a reflector sheet of a certain length along the parabola/circle form shown in Fig. 12 and measuring the distance between point 3 and 4 in Fig. 12, i.e. the width of the cover glass, and the aperture tilt,  $\beta$ , defined in Fig.12. The glass width and the aperture tilt angle were fed into the MINSUN simulation program together with the collector parameters to calculate the expected annual delivered energy. The configuration with the highest annual output is the optimum position of the reflector sheet in the parabola/circle shape. For Stockholm conditions an optimum of  $30^\circ$  aperture tilt was found. The non-symmetrical distribution of the annual irradiation leads to a lower reflector that is longer than the upper reflector.

### 2.3.3 MaReCo prototypes

Prototypes of MaReCo for stand-alone, wall and roof installation designed for Stockholm climatic conditions were built and tested at the Vattenfall Laboratory in Älvkarleby, Sweden. The designs were based on solar radiation distribution diagrams from Rönnelid and Karlsson (1997). The evaluation of the prototypes is described in Paper I.

#### 2.3.3.1 The stand-alone MaReCo

The stand-alone MaReCo for Stockholm conditions has a cover glass tilt of  $30^\circ$  from the horizontal. The collector is shown in Fig. 13. The upper acceptance angle is  $65^\circ$  and the lower is  $20^\circ$  with an area concentration of  $C_i=2.2$ . This collector is designed for stand-alone mounting on ground in large collector fields connected to a district heating system. The average operating temperature in a MaReCo field installed in a small district heating system in Torsåker, Sweden is  $65^\circ\text{C}$ .

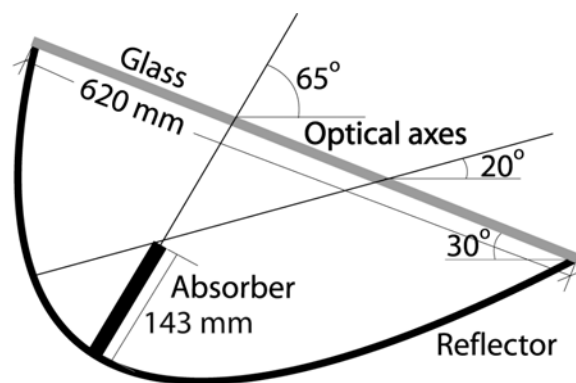


Fig. 13 Section of the stand-alone MaReCo for Stockholm conditions. Aperture tilt  $30^\circ$ . Optical axes  $20^\circ$  and  $65^\circ$  defined from the horizon.

#### 2.3.3.2 The roof integrated MaReCo

The roof integrated MaReCo shown in Fig. 14 has a smaller collector depth than the stand-alone MaReCo in order to fit on a roof connected to a heating and/or hot water system in a building. Basically the collector is designed by letting the cover glass start where the circular part of the MaReCo ends; i.e. the glass is between point 2 and 4 in Fig. 12. No upper reflector is used and the absorber is placed just underneath the

cover. The whole design is then tilted to the roof angle. All radiation from 0 to 60° angle of incidence from the cover glass normal is accepted by the reflector. The angle 60° is determined by the roof angle and the reflector thus accepts radiation from the horizon to the normal of the glass. Above 60° the collector works similar to a flat plate collector with an absorber area of 1/3 of the aperture area (the front side of the absorber). With a 30°-roof tilt the area concentration  $C_i$  is 1.5.

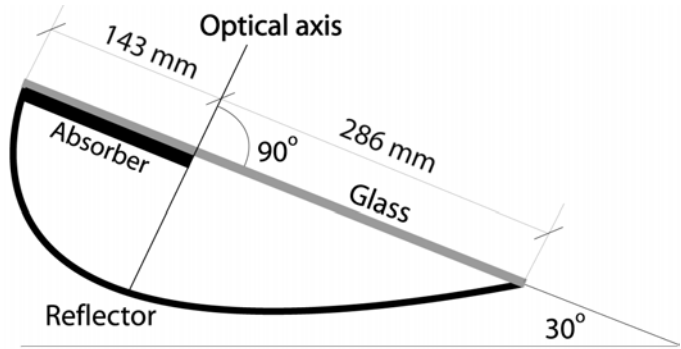


Fig. 14 Section of the roof integrated MaReCo design for a roof angle of 30°. Optical axis 90° from the cover glass.

2.3.3.3 The east/west MaReCo

All roofs in existing buildings are not aligned in the east/west direction with the roofs facing south. An alternative for roofs facing east or west is to use a specially designed roof MaReCo. In this case the reflector axis is placed in the east/west direction, tilted along the roof as shown in the photo in Fig. 15. The east/west MaReCo accepts radiation in the interval 20 to 90° from the cover glass normal as seen in Fig. 16. The area concentration is 2.0.

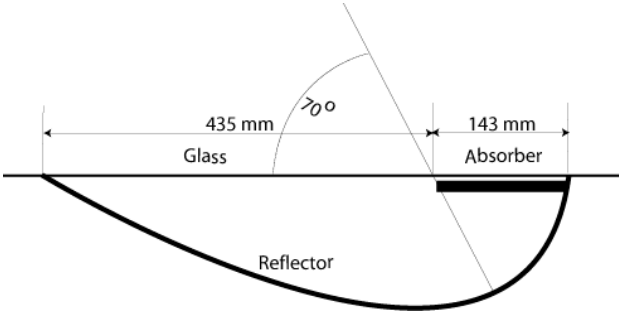
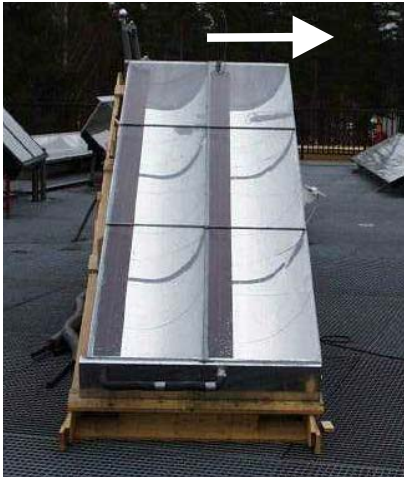


Fig. 15 Photo of a MaReCo designed for Fig. 16 Section of the east/west roof MaReCo east/west-facing roofs. The white arrow indicates the south direction. Optical axis 70° from the cover glass.

#### 2.3.3.4 The spring/fall MaReCo

Another special case of the roof integrated MaReCo is the spring/fall MaReCo. In this case a high solar fraction in the heating system over the whole year is the objective. The geometry of the collector is designed to have a high efficiency during spring and fall when the heating demand is high and a low efficiency during summer when the heating demand is low. The latter condition prevents over-heating in the system during summer. The optical axis is tilted compared to the ordinary roof MaReCo, as can be seen in Fig. 17. Beam radiation hitting the reflector at an angle smaller than  $15^\circ$  from the aperture normal will be reflected out of the collector. The absorber is placed just underneath the cover glass and it is working for all angles of incidence and not only within the acceptance interval. An area concentration of  $C_i=1.8$  is found for the spring/fall MaReCo. Another study of a season adapted concentrating collector has been made by Nordlander and Rönnelid (2001).

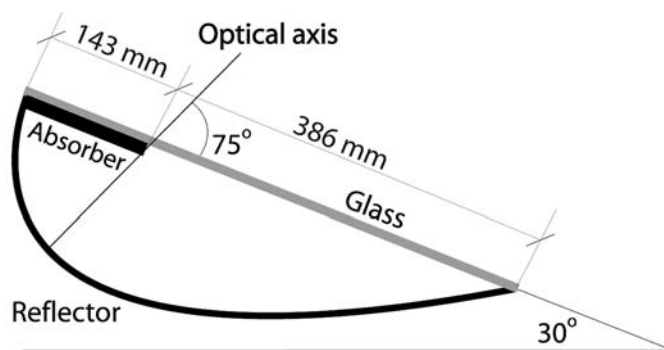


Fig. 17 Section of the spring/fall MaReCo designed for a roof tilted  $30^\circ$ . Optical axis at  $45^\circ$  from the horizon.

#### 2.3.3.5 The wall MaReCo

The wall MaReCo is an alternative to the east/west MaReCo or the spring/fall MaReCo. It can be mounted wall integrated. The concentration is  $C_i=2.2$  if both sides of the absorber are considered. The acceptance angle interval is from  $25^\circ$  up to  $90^\circ$  from the horizon as seen in Fig. 18. The absorber is placed just underneath the cover glass.

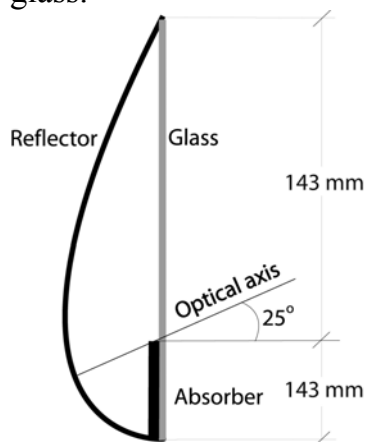
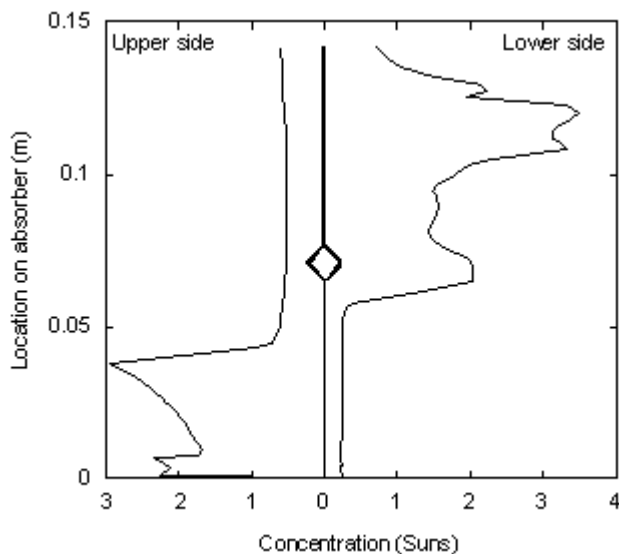


Fig. 18 Section of the wall MaReCo designed for a south facing wall. Optical axis at  $25^\circ$  from the horizon.

### 2.3.4 Characterisation of concentration distribution on the absorber fin

The radiation distribution on the absorber in a concentrating collector is in general uneven compared to the radiation distribution in a flat plate collector where the radiation is distributed evenly on the absorber. The theoretical approach to study the radiation distribution on the absorber is through ray tracing, which is described for example in Benitez et al. (1999). In Paper IV an experimental approach is suggested and a method using outdoor measurements is developed.

A monitoring device was constructed with a photo diode sliding on a potentiometer, allowing both the irradiation and position of the diode along the absorber width to be registered on a computer controlled logger. A reference photo diode was placed on the aperture of the collector. The monitoring device measured the radiation on one side of the absorber at a time. By normalising the signal from the monitoring device diode to the signal from the reference diode the actual concentration is obtained for the measured positions along the absorber width. An example of such a measurement is shown in Fig. 19 below for normal incidence (on cover glass) solar radiation. The concentration distribution,  $S_c(x)$ , shown in Fig. 19 is then measured for a series of solar radiation angles of incidence within the acceptance interval.



*Fig. 19 Concentration of normal incidence (on cover glass) radiation, on the absorber of a stand-alone MaReCo as a function of location of the radiation impact for absorber angle  $45^\circ$ . Lower side indicates facing lower reflector and upper side indicates facing upper reflector. A sketch of the absorber is drawn at zero concentration. Aperture tilted  $30^\circ$ .*

Another method to study the radiation distribution using outdoor measurements is suggested in Smyth et al. (1999) where thermocouples are attached along the width of the absorber. Fendt and Wenzel (1999) used a radiometer to study the radiation distribution on a cylindrical absorber.

### 2.3.5 Annually collected energy and optical efficiency factor

The annually collected zero-loss energy for a concentrating collector can be estimated from the concentration distribution. In an asymmetrical concentrating collector like the MaReCo the radiation is distributed unevenly on the absorber, which makes it very important to study the absorber's ability to transport the heat from the fin to the tube. If an absorber with a low efficiency is used, part of the radiation concentrated close to the edge of the absorber will be lost. To describe the efficiency of the fin in a concentrating collector the optical efficiency factor is introduced (Hellström 2001). This entity depends on the geometry and material properties of the absorber, the distance from the radiation impact to the tube and the collector overall loss coefficient. The annual optical efficiency factor can be determined from the annually collected zero-loss energy.

A method to study the annually collected energy and the annual optical efficiency factor,  $F'_{c,a}$  in a MaReCo is developed in Paper IV. The first step is to obtain the concentration distribution,  $S_c(x)$ , on the absorber at different angles of incidence for example from outdoor measurements as described in the previous section.

The concentration distribution is then multiplied by a local optical efficiency factor,  $F'_c(x)$ .  $F'_c(x)$ , gives the fraction of locally absorbed heat which is conducted to the heat carrying fluid. An example of a local optical efficiency factor distribution is shown in Fig. 20 for a stand-alone MaReCo with a fin thickness of 0.5 mm.

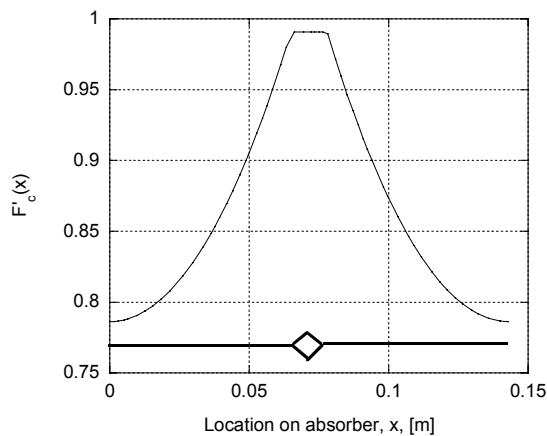


*Fig. 20 The local optical efficiency factor  $F'_c(x)$ , as a function of location  $x$  on an aluminium absorber of 0.5 mm fin thickness and a width of  $l=143$  mm for a stand-alone MaReCo with an assumed value of  $U_L=13$   $W/m^2K$  ( $U$ -value per absorber area, not aperture area) and for water at 50 °C with turbulent flow as the heat carrying medium.*

In order to obtain a measure of the total energy irradiated on the surface, a numerical rectangular method integration was performed on the irradiation data. The integration was made with and without correction for  $F'_c(x)$  since both are needed for the calculation of the annual optical efficiency factor. The numerical integration was made for each solar angle of incidence and absorber inclination angle at a time according to:

$$q_{\text{corr}}(\theta) = \sum F'_c(x)S_c(x)\Delta x \quad (48)$$

$$q(\theta) = \sum S_c(x)\Delta x \quad (49)$$

This numerically integrated and  $F'_c(x)$ -weighted energy  $q_{\text{corr}}$  is shown in Fig. 21 as the sum of the corrected energy collected from the upper and lower sides.  $q$  is the uncorrected energy collected.

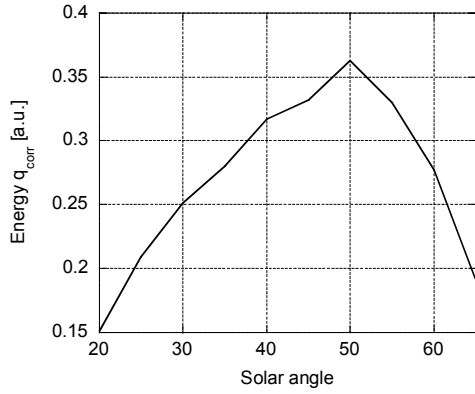


Fig. 21 Integrated and  $F'_c(x)$ -weighted energy  $q_{\text{corr}}$  at different projected solar radiation angles of incidence for absorber angle  $45^\circ$  for an absorber fin thickness of  $d=0.5\text{mm}$ . The effective concentration is obtained if the values is divided by the absorber width  $l=0.143$ .

The next step is to obtain a measure of the *annually* collected energy. In order to weight the energy at the different solar angles of incidence, knowledge of the annual irradiation distribution in the interval  $20\text{-}65^\circ$  of the meridian plane is required. This was obtained from Paper III where hourly solar beam radiation data was sorted into different angle of incidence intervals according to projected angles of incidence: the incoming energy was divided into two components, one in the north-south plane, orthogonal to the studied surface (transversal component), and one in the east-west plane, parallel to the studied surface (longitudinal component). The energy in the transversal component was sorted and summed according to projected angle into angular intervals of  $2.5^\circ$  width. They were connected to the measured angle of incidence with one interval on each side of the measured angle to a total width of  $5^\circ$  with an exception at the angular limits of the acceptance angle interval that are only  $2.5^\circ$  wide since no radiation is accepted outside these angles. The relative distribution within the interval  $20\text{-}65^\circ$ ,  $G(\theta)$ , is shown in Fig. 22.

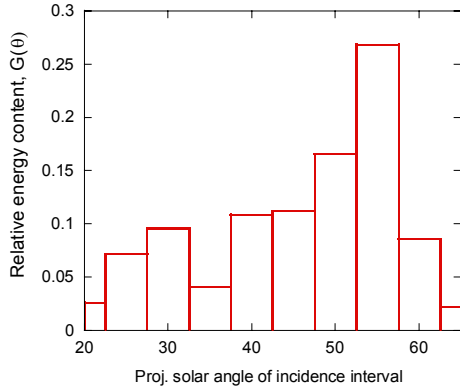


Fig. 22 Relative distribution of annually projected irradiation  $G(\theta)$  on a  $30^\circ$ -tilted plane within the interval  $20-65^\circ$  in the vertical-south plane.

Then the integrated energy is weighted by multiplying the energy at each angle shown in Fig. 21 with the relative distribution of projected annual irradiation  $G(\theta)$  in Fig. 22 and a measure of the annually  $F'_c$ -corrected collected energy,  $E_{a, \text{corr}}$  and the annually collected un- $F'_c$  corrected energy  $E_a$ , are obtained.

$$E_{a, \text{corr}} = \frac{\sum G(\theta) q_{\text{corr}}(\theta)}{\sum G(\theta)} \quad (50)$$

$$E_a = \frac{\sum G(\theta) q(\theta)}{\sum G(\theta)} \quad (51)$$

These data can then be used to calculate the annual value of the optical efficiency factor,  $F'_{c,a}$

$$F'_{c,a} = \frac{E_{a, \text{corr}}}{E_a} \quad (52)$$

A typical value of  $F'_{c,a}$  is around 0.88 for a stand-alone MaReCo with 0.5 mm thick absorber. With the same method it is also possible to calculate annual values of the concentrating collector efficiency for the incoming radiation angle by angle.

## 2.4 Projection of solar radiation

### 2.4.1 Introduction

For a flat plate collector it is possible to rotate the collector 90 degrees around the collector normal and still have the same available incoming solar radiation. For a concentrating trough-like collector this is not the case since the concentrator is designed for a certain orientation. One method to study the radiation incident on an arbitrarily oriented concentrating collector is to project the solar radiation as is described in Paper III. Related work has been done for example by Rönnelid and Karlsson (1997), Pinazo et al (1992) and McIntire and Reed (1983).

The solar radiation incident on the concentrator aperture can be projected into two components; one that is in a plane created by the concentrator axis and the normal of the cover glass, the longitudinal plane, and one component that is orthogonal to this plane, the transversal plane (Duffie and Beckman 1991). The longitudinal component of the solar radiation is parallel to the aperture area and will therefore not contribute to the energy gain of the collector. The transversal component of the solar radiation will contribute to the energy gain if the projected transversal angle of incidence is within the acceptance interval of the solar concentrator. The method starts with calculating the solar radiation component co-ordinates in the horizontal system and then the system is rotated to fit the arbitrarily oriented concentrator. Finally the projection angles in the rotated system are calculated.

Combining the method of calculating projection data with measured/calculated solar radiation data introduces the possibility of making radiation distribution diagrams, showing the available solar radiation within each projected angle of incidence interval.

#### 2.4.2 Horizontal system

The radiation components in the horizontal system  $X_0Y_0Z_0$ , seen in Fig. 23, are found through the solar azimuth,  $\gamma_s$ , and solar height,  $h_{\text{sun}}$ , according to Duffie and Beckman (1991).

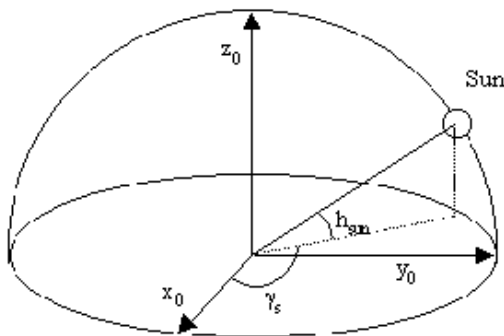


*Fig. 23 Horizontal co-ordinate system, solar height and solar azimuth.*

The solar radiation co-ordinates are then transformed from spherical to Cartesian co-ordinates,  $x_0$ ,  $y_0$  and  $z_0$ :

$$x_0 = \cos(h_{\text{sun}}) \cos(\gamma_s) \quad (53)$$

$$y_0 = \cos(h_{\text{sun}}) \sin(\gamma_s) \quad (54)$$

$$z_0 = \sin(h_{\text{sun}}) \quad (55)$$

The co-ordinate system is placed on the concentrator with the  $Y_0$ -axis along the concentrator axis as seen in Fig. 24.

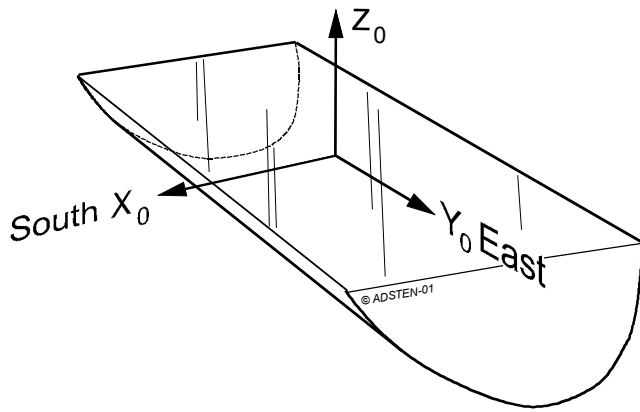


*Fig. 24 Description of horizontal co-ordinate system placement on concentrator.*

### 2.4.3 Rotated system

A rotated co-ordinate system is placed with the Y-axis,  $Y_{rot}$ , placed along the concentrator axis according to Fig. 25.

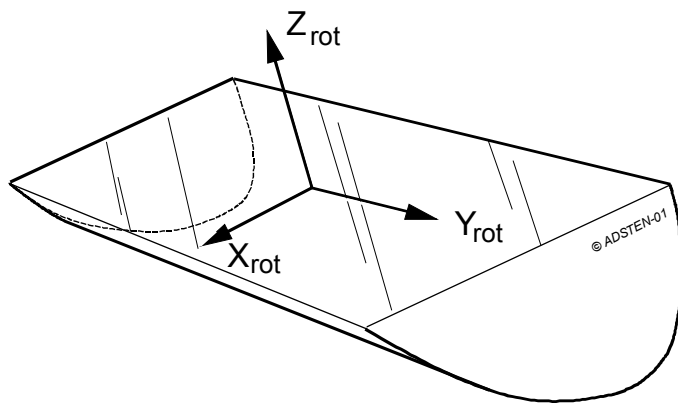


*Fig. 25 Description of co-ordinate system position on a concentrator for a rotated system.*

The rotations used here are A degrees around the X-axis, B degrees around the Z-axis and C degrees around the Y-axis, as seen in Fig. 26. The order of rotation is around X, Z and finally Y. If the concentrator is to be placed on a roof the orientation of the roof might not be exactly the optimum. With the freedom of rotating around all three axes all possible concentrator orientations can be studied.

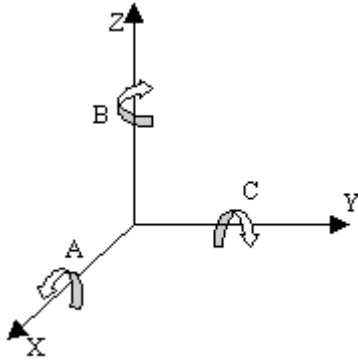


Fig. 26 Definition of rotation angles from the horizontal system.

In order to obtain the radiation component on an arbitrarily oriented surface the coordinates in the horizontal system are transformed using a rotation matrix:

$$\begin{bmatrix} x_{rot} \\ y_{rot} \\ z_{rot} \end{bmatrix} = \begin{bmatrix} \cos C \cos B & \cos C \sin B \cos A + \sin C \sin A & \cos C \sin B \sin A - \sin C \cos A \\ -\sin B & \cos B \cos A & \cos B \sin A \\ \sin C \cos B & \sin C \sin B \cos A - \cos C \sin A & \sin C \sin B \sin A + \cos C \cos A \end{bmatrix} \begin{bmatrix} x_0 \\ y_0 \\ z_0 \end{bmatrix} \quad (56)$$

#### 2.4.4 Projection angles

The solar radiation projection angles  $\theta_l$  (longitudinal) and  $\theta_t$  (transversal) are defined in Fig. 27.

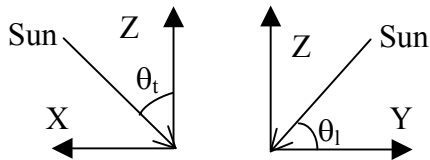


Fig. 27 Definition of solar radiation projection angles  $\theta_l$  and  $\theta_t$ .

The projection angles in the rotated system are found from the solar radiation coordinates in the rotated system:

$$\theta_t = \arctan \left[ \frac{x_{rot}}{z_{rot}} \right] \quad (57)$$

$$\theta_l = \arctan \left[ \frac{y_{rot}}{z_{rot}} \right] \quad (58)$$

#### 2.4.5 Radiation distribution diagrams

The first step to obtain a radiation distribution diagram for a surface is to calculate the solar position in the original horizontal co-ordinate system for the climate data. The earth turns 15 degrees per hour, causing large movements also in the projected angles during an hour. The hourly climate data is therefore interpolated linearly, dividing

each hour into ten intervals with constant radiation. With an improved resolution a smoother radiation distribution is obtained. The solar position co-ordinates in the original system are then used to calculate the co-ordinates in a rotated system, the projection angles and the beam radiation incident on a rotated surface. Finally the beam radiation is sorted into different projection angle intervals in 5-degree steps. An example of such a radiation distribution diagram is shown in Fig. 28 for a surface tilted  $30^\circ$  and facing south. The calculations in Fig. 28 were also made with 200 W subtracted from each hour, which is approximately the radiation needed to balance the heat losses in a concentrating collector.

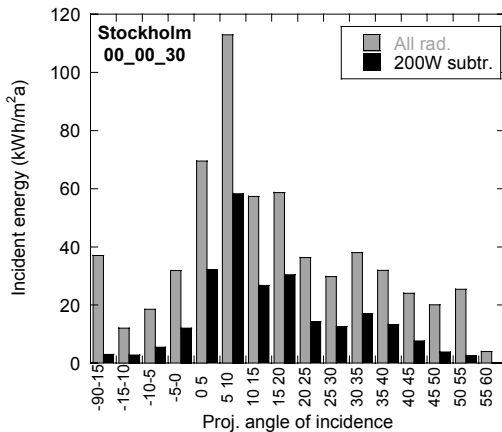


Fig. 28 Solar beam radiation distribution on a south-facing surface that is tilted  $30^\circ$  in Stockholm. Rotations  $A=0^\circ$ ,  $B=0^\circ$  and  $C=30^\circ$ . 200 W was subtracted from each hour in the radiation raw data in the black bars.

At high latitudes a large part of the annual projected solar radiation in the transversal plane is concentrated near a peak in the radiation distribution diagram around the summer solstice as seen in Fig. 28. The summer solstice peak is located at  $5.6^\circ$  solar radiation angle of incidence in the co-ordinate system that is rotated  $30^\circ$  around the Y-axis. At lower latitudes two peaks are found in the radiation distribution; one at the summer solstice and one at the winter solstice as shown by Rönnelid and Karlsson (1997). The loss of the winter solstice peak at high latitudes is due to large solar zenith angles for direct radiation during the winter months causing high absorption of the direct radiation in the atmosphere (Rönnelid et al 1996). When designing an asymmetric CPC solar thermal collector at high latitudes this means that the collector can have a small acceptance half angle covering an angular interval around the summer solstice peak, leading to a high area concentration factor according to Eq. (47).

Radiation distribution diagrams can then be used to design the acceptance interval of a CPC-collector. The same method can be used to design concentrators for PV-cells. There are several ways of designing the acceptance interval from the radiation distribution diagrams, depending on the desired properties of the concentrator. The overall principle is that adjacent projection angle energy intervals are added until the optimisation condition is fulfilled. For example the roof MaReCo described in section 2.3.3.2 has a lower acceptance angle defined by the horizon. The upper acceptance

angle is then found by adding the intervals from the horizon and upwards together until a maximum in the effective concentration is found. The effective concentration is a measure of the amount of energy reaching the absorber and is defined by:

$$C_{eff} = C_i \frac{E_{interval}}{E_{tot}} \quad (59)$$

$C_i$  is the area concentration,  $E_{interval}$  is the fraction of energy within the summed interval, and  $E_{tot}$  is the total amount of energy incident on the aperture plane. The effective concentration for different half acceptance angles is shown in Fig. 29 for the roof MaReCo.

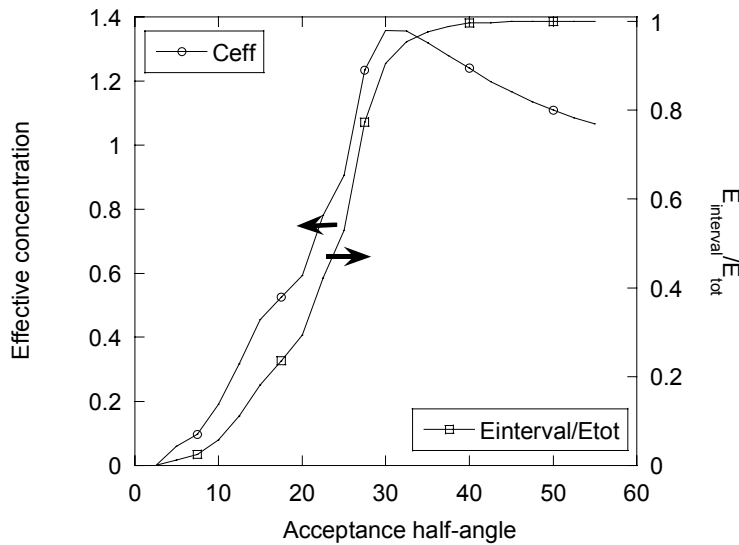


Fig. 29 Effective concentration as a function of half acceptance angle for a surface tilted 30° and facing south. The lower acceptance angle is 60 degrees in the rotated system characterised by  $A=0^\circ$ ,  $B=0^\circ$  and  $C=30^\circ$  (the horizon in the horizontal system).

The radiation distribution diagram can also be separated into different months to find the monthly distribution of the solar radiation at different projected angles of incidence as shown in Fig. 30. Note that Fig. 30 is the same case as Fig. 28 except it is divided into different periods of the year.

The monthly radiation distribution diagram can be used to determine the annual operation interval of the concentrator. As an example the roof MaReCo can be designed for a low performance during summertime to prevent overheating, the spring/fall MaReCo described in section 2.3.3.4. In this case the lower acceptance angle is the horizon in the horizontal system and the upper acceptance angle is determined from the distribution in Fig. 30 to 10°, creating a collector that reflects the major part of the radiation in May-July. The collector is still working during this part of the year since the absorber placed just underneath the cover glass is still active for the radiation hitting the absorber directly. This reduces the energy production by a factor of 3 during May-July.

Another use for the monthly radiation distribution diagrams is for design of solar shades for windows. In this case a distribution for a 90°-tilted surface facing the same orientation as the window is needed. An example of such a distribution is shown in Fig. 31 for a south facing vertical surface in Stockholm, Sweden. The length of the solar shade is then determined from the monthly distribution, depending on during which period of the year that the incoming radiation will cause over heating. To avoid the solar radiation in May-July that might cause over heating solar radiation with projected angles of incidence over 45° should be avoided. This means that if horizontal solar shades are to be installed they should have a width equal to the height of the window in Stockholm.

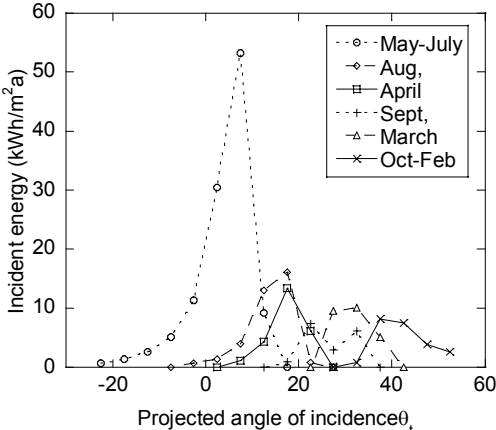


Fig. 30 Monthly distribution of the incident energy (beam radiation) for different projected angles of incidence for Stockholm on a surface tilted 30° and oriented towards south ( $A=0^\circ$ ,  $B=0^\circ$  and  $C=30^\circ$ ). 200 W subtracted from the radiation data for each hour.

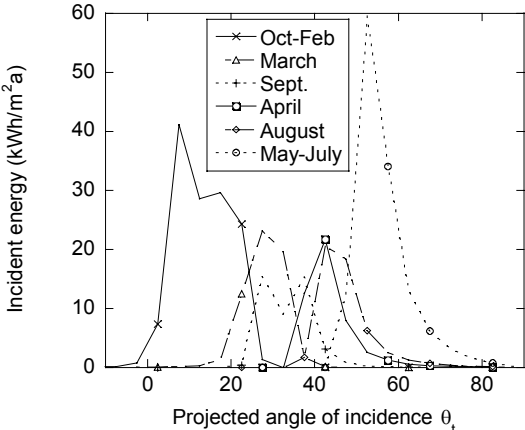


Fig. 31 Monthly distribution of the incident energy (beam radiation) for different projected angles of incidence for Stockholm on a vertical south facing surface. Projected angles defined from the horizon.

### 3 RESULTS AND DISCUSSION

#### 3.1 The MaReCo

##### 3.1.1 Evaluation of MaReCo prototypes

A total of six prototypes designed for various installation conditions were built and connected to an outdoor testing system. The tests were made according to the dynamic testing model described in section 2.1.6.6. The parameters obtained from the testing are shown in Table 1. The annually delivered energy output for each collector was simulated at an operating temperature of 50°C.

*Table 1 Estimated outputs for 50°C average operating temperature calculated with the MINSUN simulation program and investment cost per annually produced kWh for all six evaluated MaReCos.*

MaReCo Type	$Q_{50^\circ}$ kWh/m <sup>2</sup>	Cost €/kWha	$\eta_{ob}$ -	$\eta_{od}$ -	$b_0$ -	$F'U_{L1}$ W/m <sup>2</sup> K	$(mC)_e$ J/m <sup>2</sup> K
Stand-alone	253	0.61	0.59	0.37	0.37	2.4	2980
Stand-alone Teflon	282	0.55	0.64	0.36	0.46	2.2	3380
Roof integr.	336	0.46	0.69	0.56	0.29	2.4	1950
East	135	1.15	0.58	0.25	0.13	2.0	6250
West	174	0.87	0.60	0.35	0.16	2.0	4890
Spring/fall	199	0.78	0.56 0.34*	0.31 0.23*	0.41 0.23*	2.6 2.0*	2230 3800*
Wall	142	1.09	0.61	0.27	0.22	2.0	1130

\*evaluated for summer months

The study showed that all collectors have low U-values, somewhere between 1.7 and 3.2 at 50°C operating temperature depending on the type of the collector according to Table 1. This is explained by the small absorber surface compared to the total glazed area. The corresponding U-value for a flat plate collector with selective absorber is approximately from 4 W/m<sup>2</sup>K and up. An attempt was also made in the evaluation to find the second order heat loss coefficients for the collectors, but the parameter fits were better if only the first order loss coefficient was identified. The effective thermal capacitance,  $(mC)_e$  is low in most cases. This is in part explained by the low collector weight due to the low material content.

Including a teflon convection suppression film significantly reduces the losses, especially at high temperatures. The annual increase in delivered energy when including a teflon film in the stand-alone MaReCo is 29 kWh/m<sup>2</sup> at  $T_{op}=50^\circ\text{C}$ .

The roof mounted MaReCo obtained the highest annual output, 336 kWh/m<sup>2</sup> at an operating temperature of 50°C. This design can be mounted on roofs with inclination 30 ° and lower, which is an advantage compared to flat plate collectors that have an

optimum tilt of 45° for Swedish conditions. Not many roofs have a tilt of 45° in Sweden, but rather 30° or lower. The output of a flat plate collector in Sweden is around 15% higher than the output of the roof MaReCo.

The expected annual output of the east/west facing roof MaReCo is rather low. If it is facing west the annual output is however higher than that of the wall MaReCo facing south. The evaluation showed a large difference between an east/west MaReCo facing east and west. The solar radiation is symmetric around noon, but the losses are in general smaller in the afternoon since the ambient temperature is higher in the afternoon.

It is difficult to make the spring/fall MaReCo cost effective, since the material in it is the same as in the standard roof integrated MaReCo but the output is about 20% lower than the standard roof integrated version. This collector can however be used if the aim rather is a high annual solar fraction than a commercial system.

The wall MaReCo has a low annual output, only 142 kWh/m<sup>2</sup>, which is about 30% lower than that of a flat plate collector mounted on a wall. The delivered energy output is lower for any wall mounted collector but the annual distribution of the energy fits the load distribution better since the solar height is low when the demand is high. Another advantage with any wall mounted collector is that they have no problems with stagnation. The wall-MaReCo has a very special design that is appreciated by some architects.

The maximum reflector collector is designed to provide energy at a low cost. This is achieved by replacing the expensive absorber with cheap reflectors. The investment cost of the stand-alone MaReCo field shown in Fig. 32 was approximately 160 €/m<sup>2</sup>. The material content is approximately the same for all MaReCo designs even though the stand-alone MaReCo has a somewhat larger reflector area and has a need for ground supports. Using the same investment cost for all the prototypes and the outputs for  $T_{op}=50^{\circ}\text{C}$  in Table 1, the cost per annually produced kWh is calculated and found in Table 1. As seen in Table 1 the ordinary roof integrated MaReCo is the most cost efficient. A financial model, for example the annuity model, must be applied to obtain the energy cost per produced kWh. If an annuity of 0.1 is used, the cost is 0.05 €/kWh for energy produced with a roof MaReCo. This is cost effective at least compared to heat produced with electricity in Sweden, which is around 0.09 €/kWh excluding fixed costs and including tax for a household (2002). For a flat plate collector the cost per produced kWh is around 0.07 €/kWh (excluding system costs).



*Fig. 32 A field of 500m<sup>2</sup> stand-alone MaReCo collectors constructed 1999 in front of the bio fuel burner in Torsåker, Sweden. Each collector has a length of 40 meter.*

The results brought up new ideas for continued research on the MaReCo:

- A more sophisticated model for the incidence angle dependency must be used. In this evaluation only the incidence angle modifier coefficient,  $b_0$ , was identified, which is insufficient for very asymmetric collectors, such as the MaReCo. In this study  $b_0$  values of up to 0.51 are found according to Table 1, which is a bit too high to be realistic. An attempt to solve this problem using a bi-axial incidence angle modifier for the incidence angle dependency based on outdoor test data has been made by Helgesson and Karlsson (2001).
- The collectors studied here were designed from a diagram showing the energy distribution in various incidence angle intervals on a one-axis tracking south facing surface from Rönnelid and Karlsson 1997. A further study of the radiation distribution on the actual surfaces is required to investigate more accurate acceptance intervals. This study was also expanded to cover other latitudes than Swedish ones to investigate if the same concept can be used at lower latitudes. This study is described in section 3.1.3.
- Because of the asymmetry an uneven distribution of radiation is incident on the absorber. To get a high energy yield from the collector an absorber with high collector efficiency is required. A more detailed study of the radiation distribution on the absorber for various angles of incidence and absorber angles has been made in order to find a mounting with a more even radiation distribution, making the collector less dependent on the fin efficiency. This study is described in section 3.1.4.

### 3.1.2 The influence of collector components on heat losses

A study of the influence of collector components on heat losses in a stand-alone MaReCo was initiated to get more information on how to design the MaReCo as cost effectively as possible. The details of the study are found in Paper II. The study comprised absorbers with different thermal emittance, reflectors with different thermal emittance, external ventilation channels in the expanded polystyrene (EPS) and teflon film as internal convection suppression. It was also investigated if the absorber should be mounted horizontally or vertically, and the influence of having open or closed

ventilation channels in the EPS support of the reflector. The measurements were made indoors with a hot box technique as described in section 2.1.6.6. The temperature was recorded at several places in the collector box with different combinations of components. A reference collector was chosen, with a selective absorber aligned vertically, open ventilation channels, high emitting reflector, no teflon and with EPS-insulation. The most important results of the investigation are reported below.

The experiments showed measurable changes in U-value between all configurations. They also showed that the temperatures within the collector depend strongly on the actual component choice. Fig. 33 shows the influence of making one modification in the collector compared to the reference. Experiments were also made where several measures were combined, for example teflon wrapping of the absorber and a high emitting absorber.

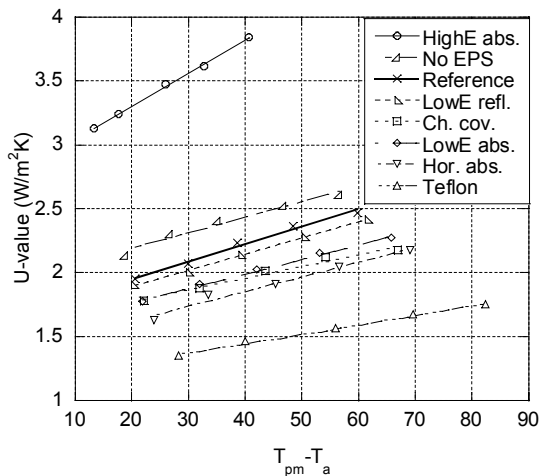


Fig. 33 U-value as a function of temperature difference between absorber and ambient for all measures. The lines show least square fits of the measurements.

Adding teflon convection suppression reduces the U-value by about 30% depending on what other modification is made at the same time. Introducing teflon is the single measure that leads to the largest improvement in U-value. Teflon film is rather cheap, 6-12 €/m<sup>2</sup>, the only problem is to design a mounting that will keep the film in position with a suitable distance to the absorber. In the MaReCo with a hot absorber area of 25% compared to that of a flat plate collector with equal aperture area, the amount of teflon needed is only half of that required in a flat plate collector. The absorber temperature is also higher than that in a flat plate collector because of the concentration.

If the absorber is placed horizontally a lower U-value is obtained compared to that obtained with a vertical mounting. The U-values are lowered by 4 to 22% with a horizontal absorber depending on what other simultaneous modification is made in the collector components. Placing the absorber horizontally leads to practically no extra costs, except for some extra supports for the absorber that might be needed to keep the absorber straight. Despite the improvement in U-value with a horizontal absorber a vertical absorber was chosen in the installed collector fields (Karlsson and Wilson 1999). One of the conclusions of this study was therefore that further investigations are

needed to find the optimal absorber angle when both optical and thermal properties are considered. This study has been made in Paper IV and is reported on in section 3.1.4.

The idea behind the ventilation channels is to reduce the risk of the EPS melting in case of stagnation. With the ventilation channels blocked the U-value was decreased by between 7 and 25% of the value obtained with open channels at 50°C temperature difference between absorber and ambient and the temperature in the upper part of the channel increased by 6°C. The channels should be designed to prevent airflow at low temperatures and reinforce the flow at stagnation temperatures since the airflow at low temperatures only causes unnecessary losses.

Using expanded polystyrene is an inexpensive way of getting the reflector in the desired geometry. It has low weight, which is an advantage especially for roof mounting and also for the transportation. A problem with EPS is that it cannot withstand high stagnation temperatures since it is only long term stable for temperatures of up to 60°C. It is also brittle and is easily damaged during transportation and installation of the collector. The measurements showed that the insulating properties of the EPS-block are not that important in the MaReCo. The increase in U-value when removing the EPS was in the interval 6 to 14% at  $\Delta T=50^\circ\text{C}$ . If the EPS was removed from the base case the U-value at  $\Delta T=50^\circ$  was increased by 8%.

A change in the collector configuration influences the temperature distribution in the collector. R1 to R4 are positions on the reflector, C1 is in the ventilation channel and A1 to A3 are air temperatures inside the collector cavity according to Fig. 34. The results are seen in Fig. 35.

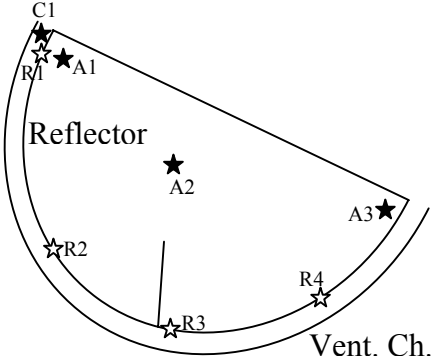


Fig. 34 Locations of investigated temperature distributions.

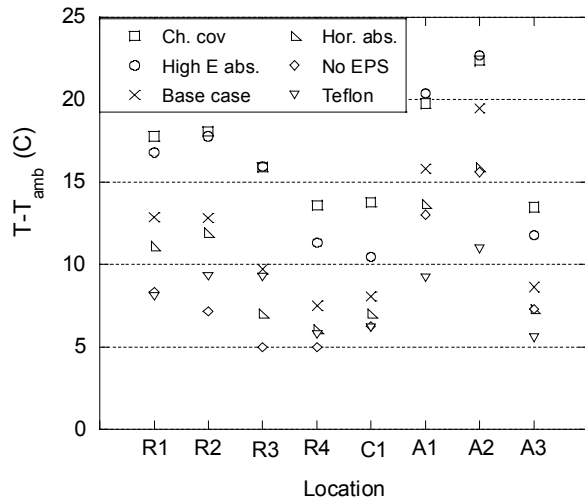


Fig. 35 Distribution of temperatures (adjusted for ambient temperature) at various locations in collector for a temperature difference of 50°C between absorber and ambient.

According to Fig. 35 the highest temperatures are found in the space in the centre of the collector cavity at location A2 in Fig. 34. Covering the ventilation channels significantly increases the temperatures in the collector but they are still below what the EPS insulation can withstand on a long-term basis according to the measurements performed here.

The stagnation temperature can be estimated from the linear loss relation in Eq. (40). If a linear fit obtained from the measurements is used for absorber temperatures above the range that is reported on here, estimated stagnation temperatures can be calculated for the different cases. It is found that in order to avoid reflector temperatures above 60°C an estimated stagnation absorber temperature for the reference configuration of 150°C and for the case with ventilation channels covered 110°C is allowed. Long term (two years) outdoor tests have shown that the EPS could endure stagnation for short periods without visible damage in spite a maximum absorber stagnation temperature of approximately 210°C. There is also some uncertainty if a linear fit from measurements in a substantially lower temperature range is valid in the stagnation region.

If teflon convection suppression is introduced the temperatures outside the teflon device are lowered. If another way of mounting the teflon would be used, the reflector temperature at the bottom of the collector could be raised. In many MaReCo installations with teflon convection suppression the teflon is mounted in a reversed V-shape over the absorber with no teflon underneath the absorber.

To summarise the results, the MaReCo should be designed with a teflon convection suppression device around the absorber. If teflon is used, a spectrally selective absorber with thermal emittance around 0.10 is quite sufficient. Horizontal absorber mounting should be used. The ventilation channels significantly change the U-value of the collector and can help to keep the reflector temperature down to protect the EPS in case of stagnation.

### 3.1.3 Theoretical optimisation of optical MaReCo design

As mentioned above one of the conclusions of the evaluation of the prototypes was that a more thorough study of the optical design was desired. The prototypes were designed from one-axis tracking south facing radiation distribution diagrams made by Rönnelid and Karlsson (1997). The new study found in Paper III featured radiation diagrams for non-tracking surfaces facing the same orientation as the apertures of the collectors. The method of obtaining the radiation distribution diagrams is described in section 2.4.5 as well as the optical optimisation procedure to design the acceptance intervals of the MaReCos.

The results of the study showed that radiation distribution diagrams is a convenient way to estimate the acceptance interval for the design of a CPC-collector. Table 2 shows the suggested acceptance intervals for different types of MaReCos for Stockholm and also the acceptance intervals of the evaluated prototypes from section 2.3.3. Note that the angles in Table 2 are defined in different co-ordinate systems according to the method described in section 2.4.3. If a detailed study of the energy accepted by the concentrator is the aim a more accurate method, for example ray tracing, is required.

*Table 2 Acceptance angle intervals, received energy and effective concentration for different designs and cities. Note that the angles are defined in different co-ordinate systems for the various MaReCo types according to the method described in section 2.4.3.*

	Lower acc. angle	Upper acc. angle	Lower acc. angle	Upper acc. angle
	Theoretical study		Prototypes	
South facing 30° inclination, stand alone MaReCo	40	0	40	-5
South facing 30° inclination, standard roof MaReCo	60	0	60	0
South facing 30° inclination, spring/fall MaReCo	60	10	60	15
West facing 30° inclination	90	15	90	20
South facing, wall	-5	-90	-25	-90

When the MaReCo design obtained with the radiation distribution diagrams is compared to the prototypes built and tested in Paper I it is found that some corrections of the acceptance angles are needed to achieve the optimum design.

The highest effective concentration is found for the stand alone application since it has two reflectors which facilitates the option to choose both limits of the acceptance angle interval. For the stand alone MaReCo a slightly smaller acceptance interval is suggested, which would increase the concentration slightly. The prototype has an acceptance interval of  $-5^\circ$  to  $40^\circ$  and the radiation distribution diagrams suggest  $0^\circ$  to  $40^\circ$ . With the

0° to 40° interval the collectable energy is reduced from 90 to 85% compared with the –5° to 40° interval.

The spring/fall MaReCo where the summer energy production is suppressed has a prototype designed with a slightly narrower acceptance interval, 15° to 60°, than that suggested by the radiation distribution diagrams, 10° to 60°. If the interval is increased more radiation in April and August, which is useful for heating, could be accepted without getting too much of the radiation in May-July, which causes over heating. With the broader acceptance interval the available solar radiation is increased from 42 to 53%.

It is also suggested that the acceptance interval of the east/west MaReCo should be expanded slightly to increase the collectable energy. The prototype had an acceptance interval of 20° to 90° and the radiation distribution diagrams suggest 15-90°, causing an improvement from 70 to 77% in the collectable radiation.

A large increase in the acceptance interval of the wall MaReCo is suggested by the radiation distribution diagrams. An upper acceptance angle of -5° instead of -25° would increase the collectable energy significantly from 65 to almost 100%. It would also expand the operating season because lower solar heights are accepted.

The alterations in geometry mentioned above can be made without increasing the costs of the collector. The method of designing the acceptance interval of a collector does not say anything about the geometry of the collector, only the acceptance interval is determined.

Two other latitudes were also studied theoretically, Madrid, Spain, (40.4°N, 3.4°W) and Munich, Germany, (48.1°N, 11.2°E). The study showed that the MaReCo design concept can be used also for these latitudes. The acceptance intervals need to be changed and the effective concentrations are in general lower compared to those for MaReCos in Stockholm. The exception is the wall MaReCo that has a higher effective concentration for the lower latitudes.

#### 3.1.4 The annually collected energy (zero loss)

The heat loss study in section 3.1.2 indicated that the U-value of the collector could be significantly decreased with an absorber aligned with the 20°-optical axis instead of the 65°-optical axis. A study, described in Paper IV and V, was initiated in order to find the optimum absorber angle from an optical point of view by studying the annually collected energy. As mentioned in section 2.3.2 the lower tip of the absorber in the stand-alone MaReCo can be placed anywhere between the optical axes. The study was made with regard to the annual solar radiation distribution to obtain the maximum energy output from the collector over the year.

A stand-alone MaReCo was constructed and the radiation distribution on the absorber was obtained with the outdoor measurement method described in section 2.3.4. The radiation distribution on the absorber for projected solar angles of incidence within the

acceptance interval, 20-65° was measured. Three different absorber inclination angles were measured, 20°, 45° and 65° from the horizon. All measurements were corrected for the optical efficiency factor and the annually collected energy was calculated according to section 2.3.5. The same set of radiation distribution measurements were used for the calculations in Papers IV and V.

In Paper IV calculations were made with absorber fins of thickness 0.5 and 1 mm and also with a 0.5mm thick fin with teflon convection suppression around the absorber. Increasing the thickness of the fin increases the optical efficiency factor. For the case with teflon convection suppression the radiation data was multiplied by 0.96 to account for the decreased transmission and the overall loss coefficient per single sided absorber area was decreased from 13 to 8 W/m<sup>2</sup>K. The results are found in Table 3.

*Table 3 Annually collected energy  $E_{a, corr}$  in arbitrary units for absorber inclination angles 20, 45 and 65° with absorber thickness  $d=0.5$  mm,  $d=1$  mm,  $d=0.5$  mm with teflon convection suppression film added.*

Absorber angle	Annually collected energy, $E_{a, corr}$ [a.u.]		
	$d=0.5$ mm	$d=1$ mm	teflon, $d=0.5$ mm
20°	0.32	0.34	0.32
45°	0.30	0.32	0.30
65°	0.26	0.28	0.27

As seen in Table 3 the maximum amount of solar radiation is collected with 20° absorber inclination angle for all three calculated cases. The amount of collected energy is increased by 18-23% with 20° absorber angle compared to that with 65° absorber angle. This result agrees with the results from the heat loss measurements in Paper II- a horizontal absorber is preferable. Increasing the absorber fin thickness from 0.5 mm to 1 mm increases the collectable energy by 6-8%. Including a teflon film around the absorber does not significantly improve the collectable energy. The reduced U-value that improves the optical efficiency factor balances the transmission loss in the teflon. The collected energy with losses considered would however be improved with the teflon.

Preliminary measurements in a solar simulator showed no significant difference between the two mounting angles, but this might be caused by the two absorber sides not having the same absorptance. New solar simulator measurements are suggested with an absorber having equal absorptance on both sides.

Another study using the annually collected energy was made in Paper V to investigate the importance of the fin width and collector geometry. Three different combinations of absorber width and collector geometry shown in Fig. 36 were investigated for absorber inclination angles 20° and 65°. The study was initiated to investigate the potential improvement with a new absorber width supplied by Sunstrip AB in Sweden. Previously a 143 mm wide absorber has been the standard, but recently a narrow fin, 71.5 mm wide, was released.

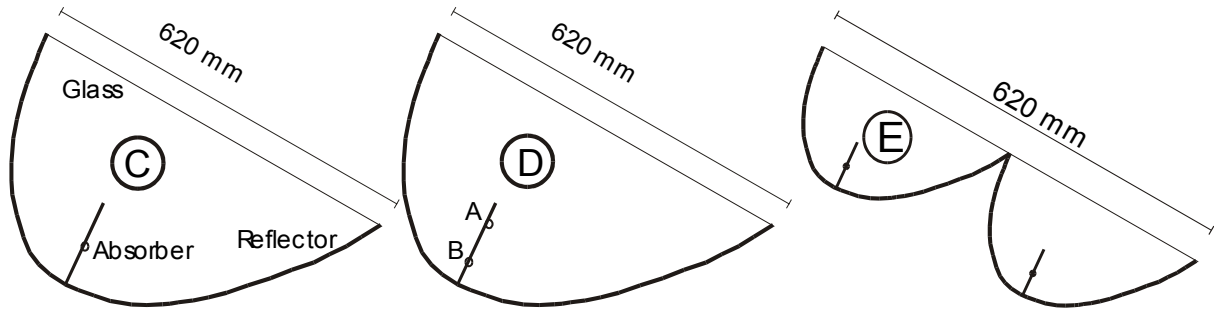


Fig. 36. Sketch of the three studied collector geometries

Configuration (C) was the standard collector also used in the study described above. Configuration (D) was a standard reflector cavity and the absorbing surface consisted of two narrow absorber fins (half of the width used in the standard collector) of thickness 0.5 mm in parallel. The two absorbers are denoted A and B where A is closest to the cavity centre. The last configuration (E) consisted of a two-unit reflector cavity with one narrow absorber of thickness 0.5 mm placed in each reflector trough. Configuration (E) was less deep than the other two. All configurations have the same absorber and aperture areas. The results of the calculations of the annually collected zero-loss energy are seen in Table 4.

Table 4 Annually collected energy  $E_{a, corr}$  in arbitrary units for absorber inclination angles  $20^\circ$  and  $65^\circ$  for the three configurations: standard wide absorber and standard reflector cavity, 2 narrow absorbers side by side in a standard reflector cavity and a 2-unit less deep reflector cavity with one narrow absorber in each cavity.

Absorber angle	Annually collected energy, $E_{a, corr}$ [a.u.]		
	C Standard absorber standard cavity	D 2 narrow absorbers standard cavity	E 1 narrow absorber less deep cavity
$20^\circ$	0.32	0.36	0.36
$65^\circ$	0.26	0.29	0.29

The configurations with narrow fins (D) and (E) collect 13% more energy at  $20^\circ$  absorber inclination angle compared to the standard configuration (C). The installed MaReCo systems have had the standard configuration (C) with the absorber mounted  $65^\circ$  from the horizon. If instead configuration (D) or (E) had been used with a  $20^\circ$  mounted absorber the annually collected (zero-loss) energy would have increased by 38%.

A more detailed investigation was made for configuration (D) to analyse the relative distribution of annually collected energy on the upper- and lower sides of the two absorbers A and B in Fig. 36. The upper side of the absorber is facing the upper reflector and the lower side is facing the lower reflector. The results of the calculations are shown in Table 5.

*Table 5 Relative distribution of annually collected energy on the upper- and lower sides of the two absorbers in configuration (D). Absorber A is placed closest to the collector cavity centre as seen in Fig. 36.*

Absorber inclination angle 20°	Abs. A upper	Abs. A lower	Abs. B upper	Abs. B lower
	29.8 %	29.6 %	19.4 %	21.2 %
	Sum 59.4 %		Sum 40.6%	
Absorber inclination angle 65°	Abs. A upper	Abs. A lower	Abs. B upper	Abs. B lower
	25.8 %	37.7 %	14.6 %	21.9 %
	Sum 63.5 %		Sum 36.5 %	

As seen in Table 5 the largest part of the radiation is collected by absorber A for both absorber inclination angles. According to Table 5 the collected energy is more evenly distributed with the 20°-mounted absorber. This leads to lower thermal losses if the absorbers are connected in parallel. If the absorbers are connected in series an uneven distribution can be an advantage. The system is then designed to first letting the water flow through the absorber with a low annually collected energy to preheat the water and then through the absorber with high annually collected energy. If one side of the absorbers in configuration (D) was to be covered by a solar cell to create a PV/thermal hybrid the 65° mounting should be used and the cell should be placed on the lower side of absorber A. This is the position receiving the maximum annual radiation.

### 3.1.5 Annual optical efficiency factor

The annual optical efficiency factor,  $F'_{c,a}$ , for the stand-alone MaReCo configuration was calculated. The method of calculating the optical efficiency factor is described in section 2.3.5. The same measurements and radiation distribution data as in section 3.1.4 was used.

In Paper IV the influence of fin thickness and teflon on the annual optical efficiency factor was investigated for three absorber inclination angles, 20°, 45° and 65°. Calculations were made for three configurations with absorber fins of thickness 0.5 and 1 mm and finally with a 0.5 mm thick fin with teflon convection suppression around the absorber. For the case with teflon convection suppression the radiation data was multiplied by 0.96 to account for the transmission through the teflon film and the overall loss coefficient per single sided absorber area was decreased from 13 to 8 W/m<sup>2</sup>K. The results are found in Table 6.

Table 6 The annual concentrating collector efficiency  $F'_{c,a}$  for a stand-alone MaReCo with absorber inclination angles 20, 45 and 65° with absorber thickness  $d=0.5$  mm,  $d=1$  mm and  $d=0.5$  mm with teflon convection suppression film added.

Absorber angle	Annual average optical efficiency factor, $F'_{c,a}$		
	$d=0.5$ mm	$d=1$ mm	teflon, $d=0.5$ mm
20°	0.87	0.92	0.92
45°	0.88	0.92	0.92
65°	0.88	0.92	0.92

As seen in Table 6 the  $F'_{c,a}$  is rather independent of absorber inclination angle. Increasing the absorber fin thickness or including a teflon film around the absorber increases the  $F'_{c,a}$  by 5-6% depending on absorber inclination angle.

The influence of absorber width and collector geometry on the optical efficiency factor was investigated in Paper V. Three different combinations of absorber width and collector geometry shown in Fig. 36 were investigated for absorber inclination angles 20° and 65°. The configurations are denoted (C), (D) and (E) and are described in section 3.1.4. The results are found in Table 7.

Table 7 Annual optical efficiency factor,  $F'_{c,a}$ , in arbitrary units for absorber inclination angles 20 and 65° for the three configurations: standard wide absorber and standard reflector cavity, 2 narrow absorbers side by side in a standard reflector cavity and a 2-unit less deep reflector cavity with one narrow absorber in each cavity.

Absorber angle	Annual average optical efficiency factor, $F'_{c,a}$		
	C Standard absorber standard cavity	D 2 narrow absorbers standard cavity	E 1 narrow absorber less deep cavity
20°	0.87	0.97	0.97
65°	0.88	0.97	0.97

According to Table 7 the two configurations with narrow absorber have an annual average optical efficiency factor that is around 10% higher than that of the standard configuration with a standard absorber.

The annual optical efficiency factor can also be calculated angle by angle,  $F'_c(\theta)$ , as seen in Fig. 37. This information can be used for example if the efficiency in a certain angle interval is important such as in the spring/fall MaReCo, where the collector with 20° absorber inclination has a higher annual optical efficiency factor, especially below 35°.

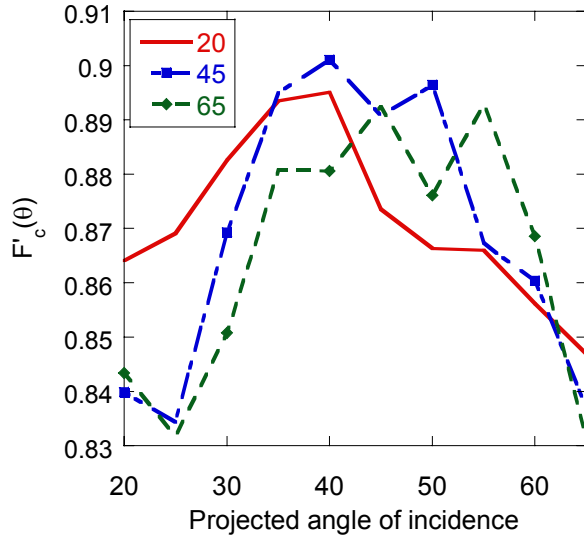


Fig. 37 Angle dependent average optical efficiency factor  $F'_c(\theta)$  for different projected angles of incidence for the MaReCo for an absorber with fin thickness 0.5 mm at different absorber inclination angles.

### 3.1.6 The influence of reflector performance on delivered energy output

In Paper VIII simulations of MaReCos with two different reflector materials were performed to investigate the influence of reflector performance on delivered energy output. In the collector fields that have been installed so far anodised aluminium reflectors have been used.

The MaReCo collector simulated in this study has an antireflection treated cover glazing and a selective absorber covered by a teflon film. The reflector in the reference MaReCo collector consisted of anodised aluminium with a total solar reflectance,  $R_t$ , of 0.85 and a specular solar reflectance,  $R_s$ , of 0.80 at 60° angle of incidence. An improved version with a silvered glass reflector with  $R_t=R_s=0.95$  was also simulated. A maximum solar acceptance angle of 65° and a minimum acceptance angle of 20° were used in the simulations. The results are listed in Table 8.

Table 8 Annual energy output and relative improvements for the MaReCo collector with a silver reflector, compared to an anodised aluminium reflector at different operating temperatures.

Op. temp. (°C)	Anod. Al output kWh/m <sup>2</sup>	Ag output kWh/m <sup>2</sup>	Relative diff. Ag-anod. Al (%)
30	377	440	16.7
50	317	377	18.9
70	269	328	21.9

The MaReCo collectors built today can be improved by 19%, if the anodised aluminium reflector is replaced by a silvered mirror. The major problem with the glass

protected silver mirror is that if it is used in the curved MaReCo geometry the glass needs to be shaped before it is coated with silver, otherwise the glass will break.

## 3.2 Flat plate collectors

Three studies concerning flat plate collectors have been made within this thesis. The first results originate from a study on how annual variations in solar radiation and ambient temperature in Sweden affect the delivered energy output from a flat plate collector. The second section describes how the delivered energy depends on the tilt and orientation of the flat plate collector in Sweden. Finally results from a study concerning the impact of the optical properties of collector components on the delivered energy output is described.

### 3.2.1 Impact of annual climate variations and location on delivered energy output

A comparative study of simulated annual delivered energy output from a solar collector using climatic data for three locations in Sweden for a sixteen year period from 1983 to 1998 was conducted in Paper VI. The aim was to elucidate the impact of climatic variations such as annual global irradiation and ambient temperature. A comparison with a synthetic year produced with Meteonorm has also been included in the study. Two different collector types were simulated, a flat plate and a vacuum tube collector. Climate data from three Swedish cities with approximately 5°-steps in latitude, Lund, Stockholm and Luleå, were used in the simulations. The simulation program MINSUN was used to perform the calculations.

Fig. 38 shows the deviation in delivered energy output from the 1983-1998 average for the flat plate collector at 50°C average operating temperature and the total radiation incident on a 45°-tilted surface and a horizontal surface for Stockholm.

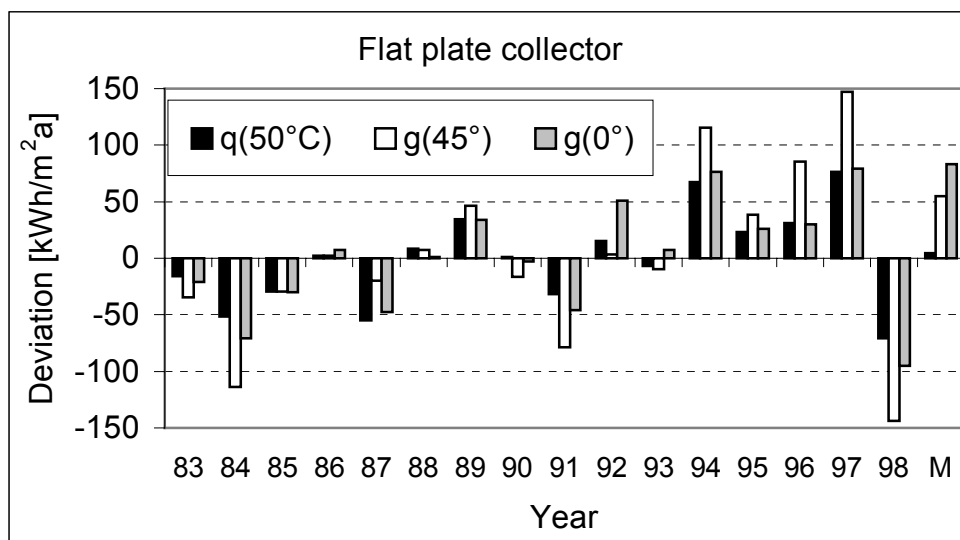


Fig. 38 Simulated solar collector output and solar irradiation on horizontal and 45°-inclined surface compared to the average output for 1983 to 1998 and a synthetic year produced with the Meteonorm weather simulation program (M) for a) a flat plate collector with high U-value for Stockholm, 1983-1998.

As seen in Fig. 38 the variations between the individual years can be rather large, the maximum deviation from the mean value is around 20% for the flat plate collector. The synthetic data obtained with the Meteonorm climate data simulation program overestimates the solar radiation compared to the 1983-1998 average, but the simulated delivered energy output is only slightly above the average. Table 9 shows average- and extreme values and standard deviations of annual solar irradiation, temperature and delivered collector energy output for collector simulations for the three Swedish cities Lund, Stockholm and Luleå.

*Table 9 Average- and extreme values and standard deviations of annual solar irradiation, temperature and collector energy output for collector delivered energy simulations for three Swedish cities. The numbers within brackets indicate the relative deviation from the mean.*

		Lund (55.72° N)		Stockholm (59.33° N)		Luleå (65.55° N)	
Average Annual irradiation on 45°-tilted surface (kWh/m <sup>2</sup> a)		1124		1113		1077	
Span insol. (kWh/m <sup>2</sup> a)		+113 (+10%)		+115 (+10%)		+146 (+14%)	
Relative highest lowest insol.		-103 (-9%)		-144 (-13%)		-126 (-12%)	
Standard deviation (kWh/m <sup>2</sup> a)		69 (6%)		77 (7%)		80 (7%)	
Average annual temperature (°C) for (G(45°)>300 W/m <sup>2</sup> )		13.4		13.6		9.8	
Temperature span (°C)		+2.1 (+16%)		+1.8 (+13%)		+1.4 (+14%)	
Relative highest and lowest		-3.3 (-25%)		-4.1 (-30%)		-1.7 (-17%)	
Standard deviation (°C)		1.3 (10%)		1.4 (10%)		1.1 (11%)	
		Flat plate Vacuum		Flat plate Vacuum		Flat plate Vacuum	
Average annual collector energy output (kWh/m <sup>2</sup> a)	T <sub>op</sub> =25°C	610	781	603	772	543	733
	T <sub>op</sub> =50°C	337	675	337	668	298	631
	T <sub>op</sub> =75°C	141	564	145	559	124	526
Span in output (kWh/m <sup>2</sup> a)	T <sub>op</sub> =25°C	-73 +84	-79 +85	-103 +113	-111 +114	-96 +91	-98 +109
	T <sub>op</sub> =50°C	-61 +65	-77 +83	-71 +76	-108	-67 +59	-95 +103
	T <sub>op</sub> =75°C	-36 +36	-59 +78	-39 +40	+112	-38 +29	-88 +94
Standard deviation (kWh/m <sup>2</sup> a)	T <sub>op</sub> =25°C	57 (9%)	55 (7%)	57 (9%)	59 (8%)	55 (10%)	61 (8%)
	T <sub>op</sub> =50°C	45 (13%)	54 (8%)	42 (12%)	58 (9%)	37 (13%)	59 (9%)
	T <sub>op</sub> =75°C	25 (18%)	53 (9%)	24 (16%)	55 (10%)	19 (16%)	54 (10%)
Relative highest and lowest							

According to Table 9 the estimated annual energy outputs for collectors placed in Lund and Stockholm are of the same order, but a collector placed in Luleå has a significantly lower expected energy output. This stresses the importance of using local climate data for the prediction of expected energy output through simulations in order not to over/under estimate the collector system.

An attempt was also made to find a simple linear model, which can be used to estimate the annual collector yield,  $q_u$  from the global irradiation on a horizontal surface,  $G(0^\circ)$  at constant operation temperature,  $T$  (given in degrees Celsius):

$$q_u = aG(0^\circ) + bT \quad (60)$$

The constants  $a$  and  $b$  are found from double-linear regression from the 1983-1998 energy output simulation data. All parameters are presented in Table 10, together with the standard deviation for each of the parameters, the  $R^2$  value and the standard deviation for the whole model.  $R^2$  is the coefficient of determination, a value between one and zero. For perfect correlation between model output and the simulated or measured values the  $R^2$ -value is equal to one.

*Table 10 Multiple linear regression to obtain parameters for  $q_u = aG(0^\circ) + bT$ , where  $G$  is the global horizontal irradiation in  $[kWh/m^2]$  and  $T$  is the average collector temperature in  $[^\circ C]$ . Regression was performed using simulated collector delivered thermal energy data for two different solar collectors with climate data for three Swedish cities, Luleå, Stockholm and Lund from 1983 to 1998.*

Coll.	City	a [-]	sd <sub>a</sub> [-]	b [kWh/m <sup>2</sup> °C]	sd <sub>b</sub> [kWh/m <sup>2</sup> °C]	R <sup>2</sup> [-]	sd <sub>model</sub> [kWh/m <sup>2</sup> ]
Flat plate	Luleå	0.86	0.011	-8.36	0.183	0.98	26
	Stockholm	0.88	0.010	-9.13	0.179	0.98	26
	Lund	0.85	0.010	-9.36	0.176	0.98	25
	All three cities	0.86	0.008	-8.82	0.142	0.97	35
Vacuum tube	Luleå	0.98	0.010	-4.22	0.157	0.95	22
	Stockholm	0.95	0.008	-4.31	0.135	0.97	19
	Lund	0.92	0.007	-4.36	0.118	0.97	17
	All three cities	0.94	0.008	-4.15	0.129	0.91	32

Fig. 39 shows a comparison between the energy outputs obtained with simulations with the MINSUN-program from climate data 1983-1998 and the proposed model from Eq (60) for the flat plate collector.

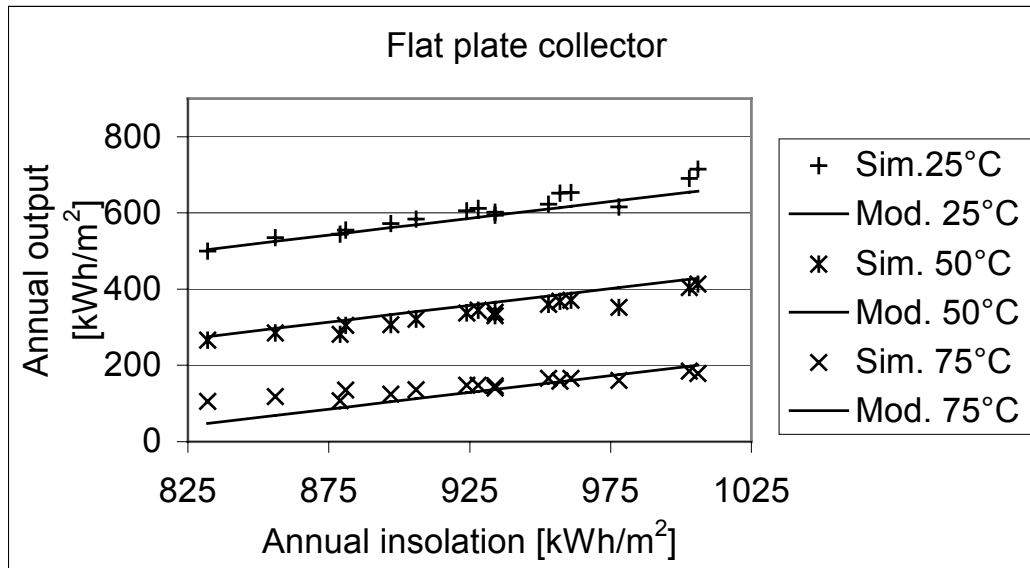


Fig. 39 Simulated, (Sim) and calculated, (Mod), solar collector thermal energy output vs. annual horizontal irradiation for a flat plate collector with high  $U$ -value. Three different average collector temperatures were simulated and calculated for Stockholm 1983 to 1998.

The delivered energy obtained with the simulated result and the double linear regression equation (Eq 51) show good agreement as can be seen in Fig. 39. Deviations are found for example for years with extreme ambient temperatures or with a very high or low beam radiation content in relation to the horizontal global solar radiation. An example of the latter is Stockholm 1992 with a high horizontal global irradiation,  $G(0^\circ)=978 \text{ kWh/m}^2\text{a}$  (average  $926 \text{ kWh/m}^2\text{a}$ ), and low beam radiation,  $G_{\text{beam}}=881 \text{ kWh/m}^2\text{a}$  (average  $972 \text{ kWh/m}^2\text{a}$ ), resulting in a too high energy output with the regression model compared to the MINSUN model. When studying Table 10 it is found that the  $a$ -coefficients (from Eq. 51) are quite close to 1, so a deviation in solar irradiation of 100 kWh leads to a change of about 100 kWh in collector delivered energy.

### 3.2.2 Impact of collector tilt and orientation on the delivered energy output

When installing solar collectors on existing buildings it is of practical importance to know how the annual performance depends on tilt- and azimuth angle. In order to obtain a reliable estimate of the expected output of a solar collector system, it is important to distinguish between the output claimed by the manufacturer, valid for a certain tilt- and azimuth angle, and the output for the actual case. In Paper VII diagrams, which can help the user to make this distinction, are developed. Different solar collectors have a different dependence on tilt- and azimuth angle. The collectors simulated were six flat plate collectors and one vacuum tube collector. Simulations for two of these collectors are presented here, one flat plate with selective absorber, low iron glass, low  $U$ -value and one vacuum tube collector of through flow type.

To investigate the influence of tilt and azimuth on collector output, a number of simulations were performed with the MINSUN program in  $10^\circ$  steps for tilt angles

ranging from 0 to 90° (horizontal to vertical) and in 30° steps for azimuth angles between +90° and -90° (west to east). Additional calculations were performed for a tilt angle of 45°, since that is often the tilt angle used by the manufacturer when predicting the performance of the collector in Sweden. The average collector temperature used was 50°C. Climate data for Stockholm, a reference year based on SMHI (Swedish Meteorological and Hydrological Institute) measurements 1983-1992, was used in the simulations. The International Energy Agency, Solar Heating and Cooling programme compiled this reference year. The Hay and Davies (Duffie and Beckman 1991) model was used for the diffuse solar radiation. Stockholm is situated on latitude 59° north and longitude 18° east. The results are found in Fig. 40 a and b.

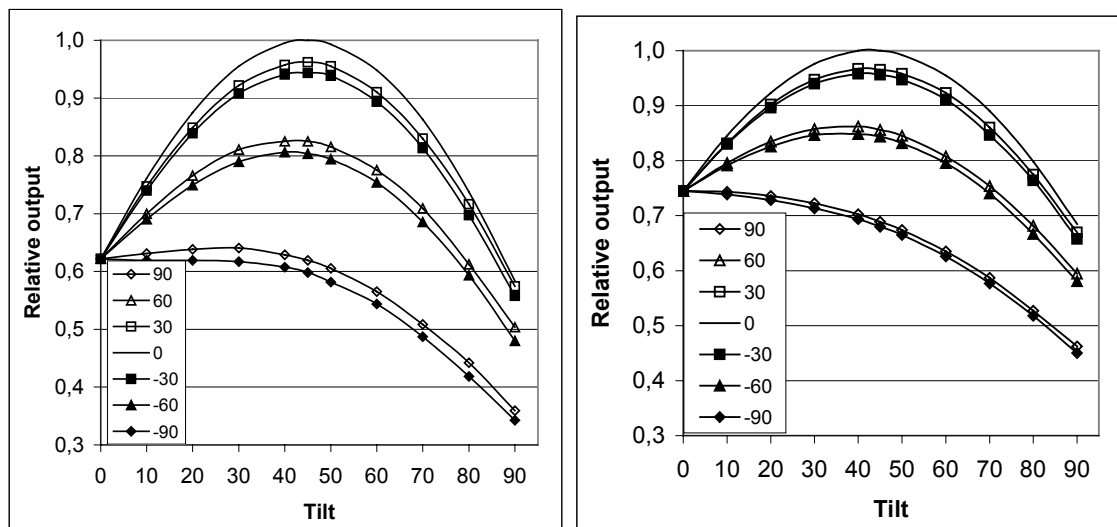


Fig. 40 a) Relative energy output for a flat plate collector with selective absorber, low U-value and low iron glass with tilt Average collector temperature 50°, maximum output 423 (kWh/m<sup>2</sup>, year).

Fig. 40 b) Relative energy output for a vacuum tube solar collector of through flow type with tilt angles 0 to 90° and azimuth angles -90 to 90°. Average collector temperature 50°C, maximum output 666 (kWh/m<sup>2</sup>, year).

There is a difference in dependence on tilt- and azimuth angle for the various collectors as seen in Fig. 40. In general non-advanced collectors have a stronger dependence on tilt- and azimuth angle and the vacuum collector, has a weaker dependency. With vacuum tube collectors there is also the possibility of tilting the absorber inside the tube during manufacturing to improve the performance for a certain tilt- and azimuth angle. Not only do the curves in Fig. 40 begin and end at different values; but the shape of the curves is also different. More advanced collectors, such as the vacuum tube collector, have a flatter structure than the simple collectors do. Optimum tilt is dependent on azimuth angle, especially for the more advanced vacuum collector. The shape of the curves and the location of the optimum tilt depend on climate and latitude.

The output for the collectors is not east- west symmetric; the output for the positive azimuth angles is slightly higher. This behaviour is more pronounced for the simple

collectors, as can be seen when comparing Fig. 40 a and b. The difference is also larger for higher azimuth angles (positive and negative) and the maximum difference is found at the optimum tilt according to Fig. 40. With the weather data used here the asymmetry is too small to be caused by variations in the radiation, but rather due to higher thermal losses in the morning due to low ambient temperatures and thermal capacity losses.

### 3.2.3 The influence of collector materials on delivered energy output

The impact of the materials properties on the energy output of solar collectors is not always well known, but with this knowledge it is possible to give priority to the most cost effective improvements. The aim of this study described in Paper VIII was to investigate the impact of material improvements of different collector components on the delivered energy output. Starting with the energy output from a “reference collector”, the impact on the energy gain due to improved absorber emittance and absorptance, adding of transparent insulation and antireflection treatment of the cover glass were evaluated. The impact of adding external or internal booster reflectors was also studied.

The calculations of the annually delivered heat were performed using the collector array model in the MINSUN simulation program. The collector parameters used in the model, for the different cases, were mainly obtained from a model based on heat transfer that calculates the temperature dependent heat loss coefficients as well as the incidence angle dependent optical efficiencies for the glazing. The model has been verified through laboratory measurements.

The reference solar collector was a flat plate collector with a spectrally selective absorber and a single glass pane with  $T_{sol}=0.90$ . For the absorber,  $\varepsilon_{therm}=0.10$  and  $\alpha_{sol}=0.95$  was chosen. No transparent insulation was included.

Eight changes from the reference case are treated (reference values within brackets):

1.  $\varepsilon=0.05$  (0.10)
2.  $\alpha=0.97$  (0.95)
3.  $\varepsilon=0.05$  and  $\alpha=0.97$ , cases 1 and 2 combined
4. Teflon film added
5. Teflon honeycomb added
6. Cover glass with structure facing the absorber
7. Antireflection cover glass,  $\tau=0.94$  (0.90)
8. Optimised collector, cases 3, 5, and 7 combined

The results and the input parameters from the MINSUN simulations are presented in Table 11.

Table 11 Absolute and relative annual energy gains ( $kWh/m^2$ ) from changes in the collector parameters for different operating temperatures and MINSUN parameters for each case.

Case			1	2	3	4	5	6	7	8
	$t_m$ (°C)	reference collector	$\varepsilon=0.05$	$\alpha=0.97$	$\varepsilon=0.05$ / $\alpha=0.97$	teflon film	teflon hc	struct. glazing	AR glazing	Optim.
Annual collector energy output ( $kWh/m^2$ )	30	608	620	621	634	606	619	594	639	672
	40	523	538	536	552	536	558	511	553	612
	50	447	464	459	477	472	501	435	476	557
	60	377	396	388	408	412	449	367	404	505
	70	313	333	324	344	357	399	305	338	455
Relative difference collector- reference (%)	30		2.0	2.1	4.3	-0.3	1.8	-2.3	5.1	10.5
	40		2.9	2.5	5.5	2.5	6.7	-2.3	5.7	17.0
	50		3.8	2.7	6.7	5.6	12.1	-2.7	6.5	24.6
	60		5.0	2.9	8.2	9.3	19.1	-2.7	7.2	34.0
	70		6.4	3.5	9.9	14.1	27.5	-2.6	8.0	45.4
MINSUN parameters (-), ( $W/m^2K$ ) ( $W/m^2K^2$ )	$F'(\tau\alpha)_b$	0.809	0.813	0.824	0.828	0.788	0.814	0.809	0.843	0.868
	$F'(\tau\alpha)_d$	0.721	0.725	0.734	0.738	0.680	0.669	0.721	0.751	0.712
	$F'U_1$	3.42	3.22	3.43	3.23	2.69	2.22	3.42	3.42	2.11
	$F'U_2$	0.0113	0.0106	0.0113	0.0106	0.0082	0.0062	0.0113	0.0113	0.0055

The presented simulations show that several improvements can be achieved for solar thermal collectors. The largest efforts should be put on the improvements that lead to the largest increase in the annually delivered energy output per cost unit. Some of the presented improvements already exist for commercial collectors, such as teflon films and antireflection treated glass. Whereas other improvements, such as an absorber simultaneously having an absorptance of  $\alpha=0.97$  and a hemispherical emittance of  $\varepsilon=0.05$ , are difficult to achieve to a reasonable cost.

By increasing the absorptance from 0.95 to 0.97 the annual energy output increases by 6% at an operating temperature of 50°C. Decreasing the emittance from 0.10 to 0.05 leads to an increase of 4% for the same operating temperature. The improvements in either absorptance or emittance for the solar absorber are realistic to obtain; some of the new commercial absorbers already exhibit these characteristics. Improvements in absorptance and emittance are possible through optimisations in the existing manufacturing process. The use of the versatile sputter depositing technique in the absorber manufacturing process increases the flexibility in comparison to previous deposition methods. It is therefore conceivable to alter the absorber coating performance without large investments.

Antireflection treated glass is commercially available for an additional cost of less than 10 €/m<sup>2</sup>. The presented simulations indicate an increase of 6% when an antireflection treated glazing, with 4% higher solar transmittance than an untreated one, is used in a collector operating at 50°C. The investigation of the structured glass, with the structure

facing the absorber, resulted in a deteriorated performance compared to the reference collector with a plane glass. In spite of this relatively poor performance, the structured glass is frequently used in Swedish solar collectors. Switching from a structured glass to a plane glass would increase the output by approximately 2%.

Including a teflon film leads to a performance increase of 6% and a teflon honeycomb to an increase of 12% at 50°C operating temperature. Including a flat teflon sheet is cost effective, especially at high latitudes and high operating temperatures. If a honeycomb of teflon is used instead the cost is too high to be cost effective, since the amount of material required is about 10 times higher than that used for a flat single film.

Adding a booster reflector in front of the collector was also investigated. In Table 12 the results from MINSUN simulations for a reference collector with a flat booster reflector are shown. Three different commercially available booster reflectors were considered; polyvinyl di-fluoride (PVF<sub>2</sub>) coated aluminium (PVF<sub>2</sub>), anodised aluminium (Anod. Al), and silver coated glass (Ag).

*Table 12 Annual energy output for the reference collector with a flat booster reflector, absolute and relative difference due to addition of a booster reflector.*

	Op.temp. (°C)	PVF <sub>2</sub>	Anod. Al	Ag
Annual energy output (kWh/m <sup>2</sup> )	30	720	770	799
	50	558	605	633
	70	421	465	492
Relative improvement with addition of reflector (%)	30	15.6	21.0	23.9
	50	19.9	26.1	29.4
	70	25.7	32.7	36.4

If the reference collector is combined with a flat booster reflector having an area twice of the collector area, an increase of 20-29% at 50°C depending on the reflector material being used is obtained. The relative improvement increases with increasing operating temperatures.

The contribution from the reflector is proportional to its specular reflectance. A second surface silver mirror is almost an ideal reflector material, with a 95% reflectance resulting in a 30% output increase. It is also relatively cheap, around 10 €/m<sup>2</sup>. The sheet of glass is however very thin, it might therefore suffer from insufficient mechanical strength. Anodised aluminium is optically fairly good with a 26% increase in output, but the long-term stability in outdoor applications is limited to about 5 years, after which the specular reflectance decreases rapidly with time. The PVF<sub>2</sub> coated sheet aluminium is a commercially produced roofing material. It is long-term stable, has good mechanical strength, and is practical to install, but has a low specular reflectance.

### 3.3 Component studies

Detailed studies were performed for two of the components in the solar collector. The first study was focused on the reflector. In this case the scattering properties of two different reflector materials were studied to investigate if a low quality cheap reflector could be used as concentrating element. The second component that was studied was the absorber. The optical constants of the absorbing layer in a Sunstrip spectrally selective absorber were investigated. If the optical constants of the layer is known it is easier to improve the coating.

#### 3.3.1 Optical scattering from rough rolled aluminium surfaces

The main reason for using external booster reflectors is to reduce the cost of energy produced with solar energy. If a cheap reflector material can be used, the system gets even more cost effective. High total reflectance in the solar wavelength range is important, and therefore aluminium and silver are the most common reflector materials used in solar energy applications. Anodised aluminium is a reflector material that is often used. High quality reflectors are specular but rather expensive compared to rolled more rough aluminium. Low-concentrating devices, such as compound parabolic concentrators (CPC) are less sensitive to scattering of the incident radiation than high-concentrating devices such as parabolic troughs or dishes. Furthermore, if the non-specular radiation is scattered in linear corrugations with a particular geometry or unidirectional rolling grooves, this can be beneficial for certain concentrator geometries.

The aim of the study in Paper IX was to examine the scattering properties of two types of cheap industrial aluminium samples with surface roughnesses originating from the cold rolling process. The first sample was sheet aluminium that looked almost completely diffuse. The second sample was an aluminium foil with quite specular appearance. The major optical difference between the two samples was the angular distribution of light scattered from the two surfaces.

The surfaces were analysed using white-light interferometry. A scan perpendicular to the rolling grooves for the sheet and the foil is shown in Fig 42.

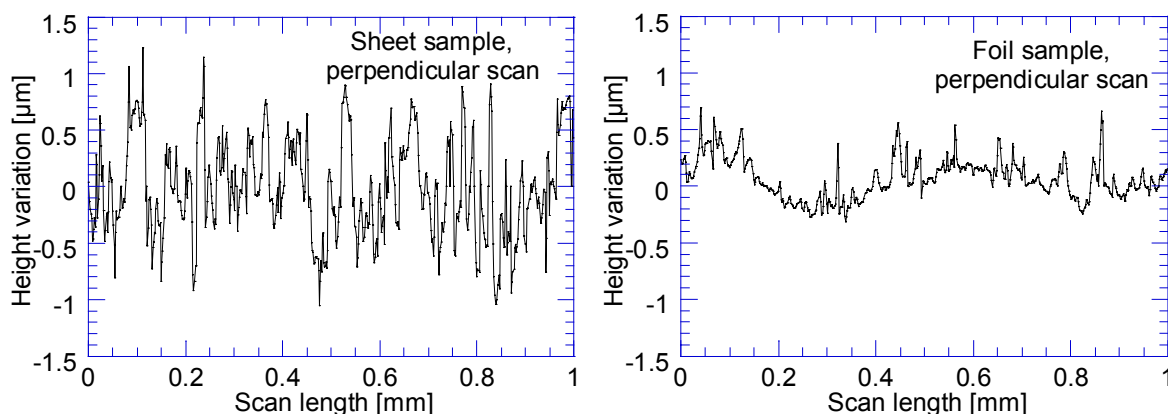


*Fig. 42 Line profiles of the aluminium sheet and foil taken with an interference fringe microscope.*

As seen in Fig. 42 the roughness of the sheet is significantly higher than that of the foil. This is manifested in a three times larger rms height for the sheet (0.6  $\mu\text{m}$ ) than for the foil (0.2  $\mu\text{m}$ ). The rms slopes were found to be gentle for both samples, thereby corresponding to large radii of surface curvature when comparing with the wavelength of the light used in the optical measurements.

The angular resolved scattering properties of the two samples were measured using ARS and TIS described briefly in section 2.1.5. The sheet was found to scatter more at higher scatter angles than the foil, as expected from the white light interferometry. Both samples have a distinct narrow band of scattered light of higher intensity extending in two directions from the specular peak. It originates from scattering by the unidirectional rolling grooves and appears as a straight line perpendicular to the grooves when these are oriented perpendicularly to the plane of the incident light. For other groove orientations with respect to the incident plane and non-normal incident light, the scatter band is bent into an arc like shape.

Using the data from the angular resolved measurements, the scatter intensity was divided into different regions according to the method of summation of scattering patterns described in section 2.1.4.2. A summary of the results is found in Table 13.

*Table 13 Scattered radiation in various angular regions (described in section 2.1.4.2). The samples are characterised by angle of incidence to the surface normal, angle of rolling grooves from the incident plane ( $0^\circ$  parallel and  $90^\circ$  perpendicular) and polarisation of light (s- or p polarised).*

Sample	SR %	LAS-B %	LAS %	HAS-B %	HAS %	Extension (band)
<b>Foil:</b>						
60°,0°,p	86.6	7.2	2.8	0.3	3.1	-11° -- +11°
60°, 0°,s	83.0	8.8	3.3	0.9	4.4	-13° -- +13°
60°,40°,p	84.7	9.3	1.2	1.8	2.2	-19° -- +15°
60°,40°,s	86.8	8.4	1.2	1.3	2.3	-15° -- +13°
60°,90°,p	73.0	19.3	1.8	4.5	1.4	-23° -- +19°
60, 90°,s	75.4	16.2	1.8	3.0	3.9	-19° -- +17°
0°,-,un-pol	74.5	14.9	2.8	3.6	4.2	-23° -- +23°
60°,90°,un-pol, (green)	75.0	18.5	1.1	2.8	2.6	-19° -- +17°
<b>Sheet:</b>						
60°,0°,p	49.6	36.7	1.6	9.1	3.0	-21° -- +21°
60°,0°,s	50.2	36.4	1.5	9.3	2.6	-21° -- +23°
60°,90°,p	28.7	37.2	0.6	29.1	4.4	-45° -- +29°
60°,90°,s	30.6	37.8	0.7	27.7	3.2	-41° -- +27°
0°,-,p	26.6	32.0	1.6	34.1	5.7	-41° -- +41°

An example of the angular distribution of scattered intensity from the sheet with light of  $60^\circ$  angle of incidence is seen in Fig. 43. The rolling grooves are perpendicular and parallel, respectively, to the incoming light in Fig. 43.

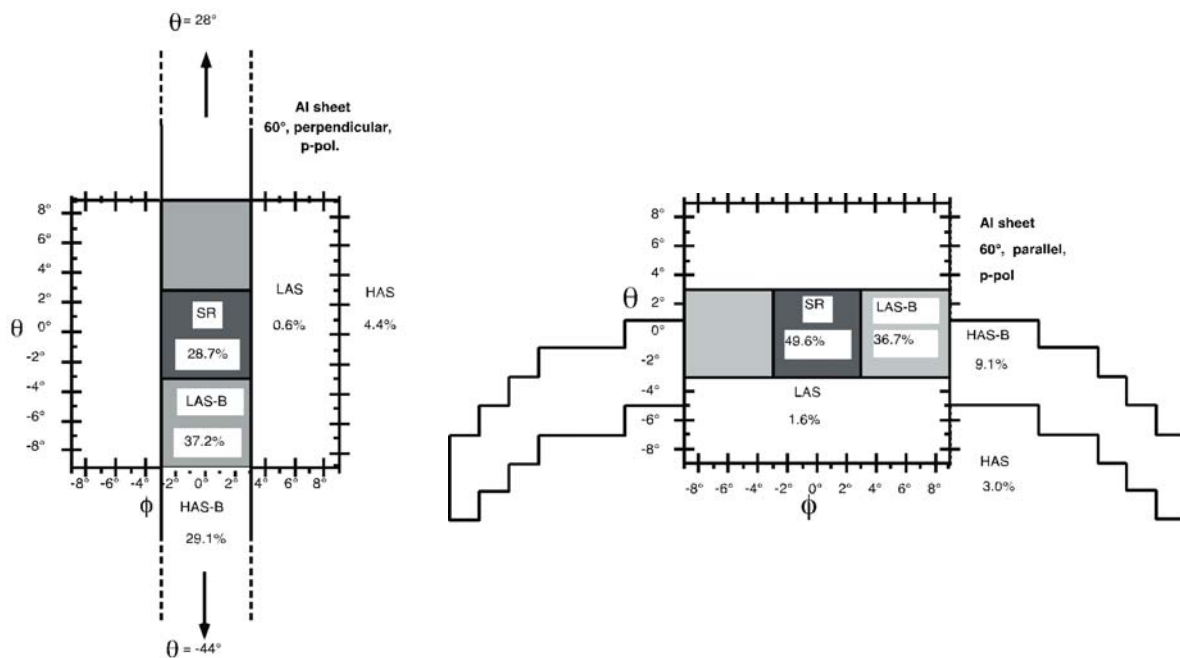
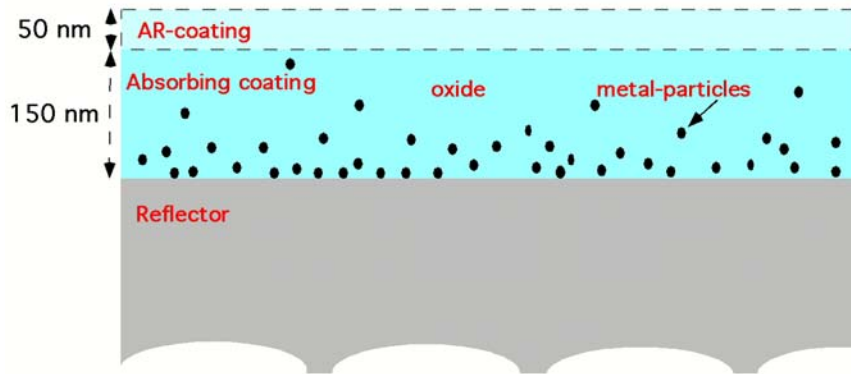


Fig. 43 Two examples of the scattering pattern from p-polarised light with a  $60^\circ$  incidence angle on the aluminium sheet. Grooves parallel and perpendicular respectively to the incident plane.

The rolled aluminium sheet, after etching, with a near normal hemispherical solar reflectance of 0.88 has a much lower specular reflectance. According to Fig. 43 it scatters almost 90% of all reflected radiation within the angular interval  $|\phi| < 9^\circ$ ,  $|\theta| < 9^\circ$  with rolling grooves parallel to the incident plane. With groove orientation perpendicular to the plane of the incident light or normal angle of incidence the specular and low angle scattering is considerably lower, about 65%. A large fraction, about 30%, is confined to the scatter band for higher angles,  $|\phi| < 9^\circ$ ,  $|\theta| < 9^\circ$ . This implies that an aluminium reflector with such a rough surface as the sheet will not perform well in a concentrating reflector application but might be acceptable as a planar booster reflector in front of flat plate solar collectors, i.e. with grooves oriented in the north south direction. As the main part of the high angle scattered light is collected in the scatter band, it will be bent downward onto the collector and will therefore give less reflectance losses than an isotropically scattering surface having the same rms height. Ray-tracing calculations for specific reflector-solar collector configurations will reveal what can be gained by using reflectors with such pronounced rolling grooves.

### 3.3.2 Optical characterisation of the absorbing layer in a nickel/nickel oxide solar selective surface

The sputter deposited Sunstrip absorber (Wäckelgård and Hultmark 1998) has been investigated in detail in Paper X. The coating shown in Fig. 41 consists of three layers, starting with a nickel barrier layer deposited on the aluminium reflector, followed by an absorbing graded index nickel-nickel oxide layer and finally an anti-reflection layer. The optical constants ( $n$  and  $k$ ) of the absorbing graded index layer were determined from reflectance, transmittance and ellipsometry data.



*Fig. 41 A model of the Sunstrip absorber in cross section showing AR-coating, absorbing coating and reflector.*

The investigated absorbing coating was deposited on a glass substrate to facilitate measurements of reflectance and transmittance of the coating. The spectral specular reflectance and transmittance were measured in a custom built spectrophotometer described in Roos (1997). These data were then fitted using a least-square method where the  $n$ - and  $k$ -values were fitted simultaneously. A two-layer structure was used in the model. This is a too simple model for a graded index coating, but provides some information about the optical constants of the base and top parts of the coating.

It was found that the top part of the graded index layer has a refractive index that increases monotonically from  $n=1.7$  to  $n=2.5$  and a constant extinction coefficient of  $k=0.5$  over the measured spectral range. The base part of the graded index layer has a metallic behaviour with higher  $n$ - and  $k$ -values than the top part and they were found to increase with wavelength. A further optimisation of the sputter deposition process is taking place at the moment but without the participation of the author.

## 4 CONCLUSIONS AND SUGGESTION FOR FUTURE WORK

The thesis comprises system aspects on solar collectors and how system performance is linked to thermal and optical properties of the materials in the collector components.

The MaReCo design has the potential to provide energy at a low cost, achieved by replacing the expensive absorber with cheap reflectors. A large part of the available solar radiation can be collected without the need for tracking, which would increase the investment and maintenance costs. The MaReCo design concept is flexible and can be adapted to various installation conditions. The evaluation of the prototypes in Paper I shows that all MaReCo types function as expected. The highest annually delivered energy output was found for the roof mounted MaReCo. Based on this evaluation an estimated investment cost of 0.46 € per annually produced kWh for the roof integrated MaReCo and an annuity of 0.1, leads to an energy cost of 0.05 €/kWh. This is cost effective in Sweden, at least compared to the electricity price, which is around 0.09 €/kWh including tax for a household (excluding fixed costs). The cost effectiveness can be further increased through the results found in this thesis.

The major suggested improvements in components and system performance to increase the performance are listed in the following:

- Paper I, Paper II and Paper IV show that the use of *teflon* is recommended in the MaReCo since the absorber temperature is significantly higher than that of a flat plate as an effect of the concentration
- The studies of the *absorber inclination angle* all show that the absorber should be mounted along the 20°-optical axis both from a thermal and an optical point of view. The installations so far have been made with the absorber mounted along the 65°-optical axis. Further studies of this are suggested, for example an outdoor test with two identical prototypes but with different absorber inclination angle.
- An improvement in the geometry of the MaReCo is possible through a slight correction of the *acceptance interval* compared to the prototypes as shown in Paper III. For the wall MaReCo a change in the lower acceptance angle from 25° from the horizon to 5° would increase the collectable fraction of the incoming solar radiation from 65% to almost 100%.
- In a non-imaging concentrator a *reflector* material that is not completely specular might be used. Paper IX involves a study of an aluminium foil laminated with plastic, which might be a good enough reflector for the MaReCo. It is cheaper than the anodised reflector most frequently used in the MaReCo. A study linking Paper IX with Paper IV is therefore suggested where the radiation distribution on the absorber is studied for a MaReCo with a reflector of foil laminated with plastic. A rougher sheet metal was also studied in paper IX, but it was concluded that this material scattered too much to be used in internal reflectors in concentrating

collectors but could be used in external booster reflectors for flat plate collectors. Another way to increase the delivered energy output is to increase the solar reflectance of the reflector. As mentioned in Paper VIII the delivered energy output is significantly increased if the anodised aluminium is replaced by silvered glass.

- The *ventilation channels* investigated in Paper II can prove to be important in case of stagnation for the MaReCo with EPS-insulation. The reflector is resting on the EPS-insulation, which is not long-term stable for temperatures above 60°C. The channels significantly help to lower the reflector temperature.
- A *thicker absorber fin* is suggested from measurements and calculations of the annual incident solar radiation on the absorber in a stand-alone MaReCo. With an absorber fin of 1 mm thickness instead of 0.5 mm 5% more energy is collected. If the *narrow absorber fin* of width 71.5 mm is used instead of the standard absorber (143 mm) 13% more energy can be collected at absorber inclination angle 20°. If the standard configuration used in the present installations with 143 mm wide absorber and 65° absorber angle is compared to using the narrow 71.5 mm absorber mounted at 20°, 38% more energy can be collected.

A method to obtain an estimate of the acceptance interval for the design of a CPC-collector from radiation distribution diagrams was developed. The method worked very well for the MaReCo and it is also applicable for the design of the acceptance interval of any CPC-collector.

The method of measuring the concentration distribution on the absorber of a concentrating collector and then calculating the collected energy and annual optical efficiency factor developed in Paper IV worked very well. The method does not require sophisticated equipment and a lot of information about the collector can be obtained from one set of measurements. In the measurements described in Papers IV and V angles within the acceptance interval were investigated. If angles outside the acceptance interval were measured the incidence angle dependency of the collector could be obtained. The major part of the energy is within the acceptance interval, but some radiation is also accepted outside the acceptance interval.

The simulations of annual performance of flat plate collectors were performed to investigate the impact of tilt, azimuth and annual climate variations on collector performance. When solar collectors are tested at the Swedish National Testing and Research Institute, SP, the results are valid for the optimum tilt (45°) and azimuth (0°) and simulated with a standard climate for central Sweden. According to Paper VII there is a large variation in delivered collector energy output for different tilts and azimuths. If the roof tilt is within 30-60° and the azimuth within  $\pm 30^\circ$  the delivered collector energy output is at least 90% of that for the optimum conditions according to Paper VII. Advanced collectors, such as vacuum tube collectors, depend less on tilt and azimuth compared to less advanced collectors such as a flat plate collector with a non-selective absorber. There is also a large variation in delivered collector energy output between southern/central and northern Sweden according to Paper VI. Owing to

these factors the amount of energy that the individual owner gets from his solar collector can therefore be significantly different from the test results. The annual climate variations have a large impact on the solar collector as found in Paper VI. If a 16-year average in collector delivered energy obtained from simulations with measured climate data is compared to the maximum and minimum annual energy production, deviations of up to 100 kWh/m<sup>2</sup> are found. There is also a large difference between the estimated average delivered energy output between northern Sweden and mid/southern Sweden. For a flat plate collector with selective absorber, a collector placed in Luleå has an estimated delivered energy output that is 88% of that of a collector placed in mid/southern Sweden.

The investigations of the impact of the materials in the collector components on the delivered energy output showed that a lot of improvements are possible. It is especially important to link the performance increase with the cost of the improvement. The study in Paper VIII showed that using anti reflective treated cover glass, including teflon and adding a flat external booster reflector are measures that are cost effective for flat plate solar collectors.

Finally, it is of interest to compare the MaReCo with the flat plate collector. The simulated flat plate collector is a large area collector with teflon and a low U-value,  $\eta_{ob}=0.75$ ,  $\eta_{od}=0.60$ ,  $F'U_1=3.5$  W/m<sup>2</sup>K,  $F'U_2=0.002$  W/m<sup>2</sup>K<sup>2</sup>,  $b_0=0.19$  and  $(mC)_e=6$  J/m<sup>2</sup>K. The present MaReCo is approximately the stand-alone MaReCo from the prototype evaluation in Paper I except the  $b_0$  value is decreased from 0.37 to 0.30. A future MaReCo with some of the improvements suggested in this thesis is introduced. The process of obtaining the parameters for the future MaReCo is described below.  $(mC)_e=3$  J/m<sup>2</sup>K,  $b_0=0.30$  and  $F'U_2=0$  are assumed to be the same for the present and the future MaReCo. The relative decrease in the real U-values is assumed to be the same as that for the laboratory value and the increase in  $F'$  is assumed to be the same as that of  $F'_{c,a}$ .

The present MaReCo:

$$\eta_{ob}=0.60$$

$$\eta_{od}=0.40$$

$$F'U_1=2.4$$

1. Introducing *teflon*. The laboratory U-value is lowered from 2.4 to 1.5 according to Paper II. The transmittance is decreased with 0.96. The annual optical efficiency factor,  $F'_{c,a}$ , is increased from 0.88 to 0.92 according to Table 6. The collectable energy is increased from 0.26 to 0.27 a.u. in Table 3, the same increase is assumed for  $\eta$ .

$$\eta_{ob}=0.60 \times 0.96 \times (0.27/0.26) = 0.60 \quad \eta_{od}=0.40 \times 0.96 \times (0.27/0.26) = 0.40 \quad F'U_1=2.4 \times (1.5/2.4) \times (0.92/0.88) = 1.6$$

2. Changing the *absorber inclination angle* to 20°. The decrease in laboratory U-value is from 1.5 to 1.4 from Paper II. The  $F'_{c,a}$  is the same according to Table 6. The collectable energy is increased from 0.27 to 0.32 a.u. in Table 3.

$$\eta_{ob}=0.60 \times (0.32/0.27) = 0.71 \quad \eta_{od}=0.40 \times (0.32/0.27) = 0.47 \quad F'U_1=1.6 \times (1.4/1.5) = 1.5$$

3. Using *two narrow absorber fins* instead of one wide. Configuration D in section 3.1.4 is used, the heat losses are assumed not to be affected. Changing to a narrow absorber increases the  $F'_{c,a}$  from 0.87 to 0.97 according to Table 7. This is without teflon, so the  $F'_{c,a}$  is instead approximated to increase from 0.92 to 0.97. The increase in  $\eta$  is assumed to be the same as the increase in  $F'_{c,a}$ .

$$\eta_{ob}=0.71 \times (0.97/0.92) = 0.75 \qquad \eta_{od}=0.47 \times (0.97/0.92) = 0.50 \qquad F'U_1=1.5 \times (0.97/0.92) = 1.6$$

Table 14 shows simulations made with the MINSUN program of the annually delivered energy output of a flat plate collector and a stand-alone MaReCo.

*Table 14 Annually delivered energy output for a flat plate collector and a MaReCo.*

Temperature	Flat Plate [kWh/m <sup>2</sup> ]	Present MaReCo [kWh/m <sup>2</sup> ]	Ratio Pres. MaReCo/ Flat Plate	Future MaReCo	Ratio Fut. MaReCo/ flat plate
25°	579	378	0.65	496	0.86
50°	401	289	0.72	411	1.02
75°	271	224	0.83	348	1.28

According to Table 14 the performance of the flat plate collector is higher than that of the present MaReCo. The low U-value of the MaReCo is an advantage especially at high temperatures as seen in Table 14, the ratio between the performances of the two collectors increases with temperature. For the future MaReCo the performance is higher than that of the flat plate for operating temperatures of 50° and 75°. The parameters used in the simulation are obtained in a theoretical study, and the interaction of some of the improvements is not known. It does, however, show that there is a potential for improvement to a performance that is in the same range as the flat plate collector at 50° operating temperature and perhaps an even better performance at higher temperatures.

The MaReCo has a lower investment cost compared to the flat plate collector. There is also a potential for further cost reduction for the materials in the MaReCo, especially the reflector. The MaReCo design is flexible with possibilities to design the collector for various installation conditions or special demands. Examples of this are the east/west MaReCo and the spring/fall MaReCo. Because of the low materials content, the MaReCo is light, which is an advantage for roof mounting. As of today, the roof MaReCo has a larger collector depth than the flat plate, but this can be reduced with the use of the new 71.5 mm wide absorber. The same principle of MaReCo design can be used for thermal and PV applications. The particular design of the MaReCo might be a problem from an aesthetic point of view, some architects like it and others do not.

The major advantages with the flat plate collector is its higher performance and that it is well established among manufacturers and customers. There is also plenty of experience of the long-term performance of the flat plate collector.

## 5 SUMMARY OF APPENDED PAPERS

### Paper I Evaluation of asymmetric CPC-collector designs for stand-alone, roof- or wall integrated installation

The *Maximum Reflector Collector*, MaReCo, is a heavily truncated and non-symmetric compound parabolic concentrator (CPC) extended in the east-west direction with a bi-facial absorber optimised for northern latitudes. The MaReCo concept is flexible and can be used for different applications. In this paper MaReCos for stand-alone, roof and wall mounting are studied. Prototypes of six different MaReCos have been built and outdoor-tested. The evaluation gave the highest annual energy output for the roof mounted MaReCo, 336 kWh/m<sup>2</sup> and the stand-alone MaReCo with teflon 282 kWh/m<sup>2</sup> at an operating temperature of  $T_{op}=50^{\circ}\text{C}$ . A special design for roofs facing east or west was also investigated, and gave an annual energy output of 135 (east) and 174 (west) kWh/ m<sup>2</sup> at  $T_{op} =50^{\circ}\text{C}$ . If a high solar fraction over the year is the objective a MaReCo with a high output during spring/fall and a low output during summer can be used. Such a collector had an output of 199 kWh/ m<sup>2</sup> at  $T_{op}=50^{\circ}\text{C}$ . Finally a MaReCo for wall mounting was evaluated, with an expected output of 142 kWh/ m<sup>2</sup>a at  $T_{op}=50^{\circ}$ .

### Paper II Calorimetric measurements of heat losses from a truncated asymmetric solar thermal concentrator

Indoor heat loss measurements have been performed on a truncated asymmetric compound parabolic concentrating collector with concentration  $C=2.2$ . An electrically heated flat bi-facial absorber aligned in the east-west direction was used. Geometrical and material properties that affect the heat losses were investigated. The reference configuration was a collector with polystyrene insulation, anodised aluminium reflector, acrylic plastic cover and a vertically mounted selective absorber. The components in the reference configuration were then modified. The modifications were high-emitting black painted non-selective absorber, low-emitting un coated aluminium absorber, adding teflon transparent insulation, low-emitting aluminium reflector, placing the absorber in horizontal position, covering ventilation channels in the polystyrene insulation and removing the back insulation. The measurements show significant differences in U-value for almost all configurations. Adding a teflon film is the single modification that causes the largest improvement in U-value, 35-55%, mounting the absorber horizontally instead of vertically lowered the U-value by up to 22%, replacing the selective absorber by a high-emitting absorber increases the U-value by 73%, and using a low-emitting absorber lowers the U-value by 11% compared to the selective absorber. All values presented at  $\Delta T=50^{\circ}$ . The ventilation channels constructed to protect the insulating block from overheating increases the U-value by 7-22%. The variations in collector temperature distribution when the material and geometrical properties were altered were also studied.

### Paper III Annually projected solar radiation distribution analysis for optimum design of asymmetric CPC

A method to study the projected solar radiation angle of incidence distribution on an arbitrarily oriented surface is suggested. The method is based on a projection of the incident solar radiation onto two orthogonal planes, one created by the concentrator axis and the normal of the cover glass and one created by the orthogonal of the concentrator axis and the cover glass normal. For a two-dimensional concentrator the component orthogonal to the concentrator axis is the only component of interest since the other component is parallel to the cover glass. Solar radiation distribution diagrams are made for three cities, Madrid Spain, Munich Germany and Stockholm Sweden for four different surface orientations. The radiation distribution diagrams can be used to roughly design the acceptance interval of a solar concentrator. This method is used to design the acceptance interval of the *Maximum Reflector Collector*, MaReCo, a two-dimensional asymmetric CPC specially designed for high latitudes (Stockholm). It can be designed for various installation conditions, on ground, roof or wall. Prototypes of the MaReCo have previously been built and tested. In this work it is investigated if the prototype designs are consistent with the designs obtained from the radiation distribution diagrams. The existing prototypes could, with the exception of the roof MaReCo, be improved with slightly changed acceptance intervals. It is also investigated if the same design principle can be used for somewhat lower latitudes, i.e. Munich and Madrid. The study shows that the MaReCo design principle can be used for lower latitudes with a small decrease in the concentration factor.

### Paper IV Measurement of radiation distribution on the absorber in an asymmetric CPC collector

A method to estimate the annually collected energy and to calculate the annual average optical efficiency factor is suggested. The radiation distribution on the absorber of an asymmetric CPC collector with a flat bi-facial absorber is measured for three different absorber inclination angles using a photo diode. The annually collected energy and annual optical efficiency factors are determined for collectors with absorber fin thickness 0.5 mm and 1 mm and for a collector with a teflon convection suppression film mounted around the absorber. With the local optical efficiency factors and the annual incident solar energy distribution considered, the energy gain without losses for a mounting angle of 20° is 21-22% higher than for a collector with 65° absorber inclination angle. The annually collected energy is increased with 6-8 % if the absorber fin thickness is increased from 0.5 to 1 mm. The annual average optical efficiency factor is relatively independent of absorber inclination angle. It was found to be 0.87-0.88 for a collector with a 0.5 mm thick absorber fin and 0.92 for a collector with a 1 mm thick absorber fin or for a collector with 0.5 mm thick absorber fin with a teflon convection suppression film added.

## Paper V Comparison of the optical efficiency of a wide and a narrow absorber fin in an asymmetric concentrating collector

For a compound parabolic concentrating collector with a certain design a wider absorber leads to a larger collector depth. The aim of this study was to investigate the optical efficiency of three different combinations of absorber width and reflector cavity depths for an asymmetrical truncated concentrating thermal collector designed for ground mounting. Outdoor measurements of the radiation distribution on the absorber fin are used to calculate the zero-loss annually collected energy and average optical efficiency factor. Three different configurations of reflector geometry/absorber width were investigated: A reference case with a standard fin and one deep reflector cavity, (C), two narrow fins side by side and one deep reflector cavity, (D), and finally two less deep reflector cavities with one narrow absorber fin each, (E). Two different absorber mounting angles were investigated, 20 and 65° from the horizon. The calculations show that with the absorber mounted 20° from the horizon the annually collected energy (zero-loss) increases by 13% if any of the configurations (D) or (E) with narrow fins are used. The annual average of the optical (zero-loss) efficiency factor increases by approximately 11% for both the configurations (D) and (E) with narrow fins, compared to the reference case (C). If the collected energy with configuration (C) with 65° absorber angle, which has been used in installed collector systems of this kind, is compared to that of configurations (D) or (E) with 20° absorber angle, an increase of 38% is found.

## Paper VI The influence of climate and location on collector performance

The influence of annual climate variations on the performance of solar thermal collectors in the northern part of Europe has been investigated. The annual solar collector energy output has been calculated with the MINSUN simulation program using hourly, measured climatic data for the years 1983 to 1998 for three cities situated in the south (Lund), central (Stockholm) and north (Luleå) of Sweden. A synthetic year created with the Meteonorm weather simulation program was also used in the simulations. Two solar thermal collectors were modelled: a flat plate solar collector and a tubular vacuum collector, both of commercial standard. The annual average energy delivered from the flat plate collector was 337 kWh/m<sup>2</sup> for Stockholm (337 for Lund and 298 for Luleå), and from the vacuum tube collector 668 kWh/m<sup>2</sup> for Stockholm (675 for Lund and 631 for Luleå) at an operating temperature of T=50°C. Maximum deviations from the average value for this sixteen year period are around 20% for the flat plate and 15% for the vacuum tube collector, at T=50°C. The relation between global irradiation on a horizontal surface and the annually collected thermal energy at a constant operating temperature could be fitted to a linear equation:  $q_u = aG(0^\circ) + bT$ .  $q_u$  is the energy output from the collector,  $G(0^\circ)$  the global irradiation at a horizontal surface, T the average temperature of the collector fluid and  $a$  and  $b$  fitting parameters in a double linear regression analysis.

## Paper VII Simulation of the influence of tilt and azimuth angles on the collector output of solar collectors at northern latitudes

For solar collector systems it is important to estimate the energy gain of the system for an actual case from the specification provided by the manufacturer, valid for a certain tilt- and azimuth angle. The performance for tilt angles between 0 and 90° and azimuth angles between +90 and -90° (west to east) in steps of 10° have been simulated. The simulation tool used is the MINSUN model (Chant 1985). Weather data for Stockholm were used. Different solar collectors have a different dependence on tilt angle and azimuth angle. In general a more advanced solar collector has a weaker dependence on tilt- and azimuth angle since the thermal losses are smaller. According to the simulations presented here the flat plate with non selective absorber has the strongest dependence on tilt- and azimuth angle and the vacuum tube collector of the through flow type has the weakest dependence. If the roof tilt is within 30-60° and the azimuth within  $\pm 30^\circ$  the delivered collector energy output is at least 90% of that for the optimum conditions.

## Paper VIII The impact of optical and thermal properties on the performance of flat plate solar collectors

The impact of the optical properties on the annual performance of flat plate collectors in a Swedish climate has been estimated with the MINSUN program. The collector parameters were determined with a theoretically based calculation program verified from laboratory measurements. The importance of changes in solar absorptance and thermal emittance of the absorber, the addition of a teflon film or a teflon honeycomb, antireflection treatment of the cover glazing and combinations of these improvements were investigated. The results show that several improvements can be achieved for solar thermal absorbers. A combined increase in absorptance from 0.95 to 0.97 and a decrease in emittance from 0.10 to 0.05 increase the annual performance with 7% at 50°C operating temperature. The increase in performance by installing a teflon film as second glazing was estimated to 6% at 50°C. If instead a teflon honeycomb is installed, a twice as high performance increase is obtained, 12%. Antireflection treatment of the cover glazing increases the annual output with 6% at 50°C. A combination of absorber improvements together with a teflon honeycomb and an antireflection treated glazing results in a total increase of 25% at 50°C. Including external booster reflectors increases the expected annual output at 50°C to 20-30% depending on reflector material.

## Paper IX Optical scattering from rough aluminum surfaces

Bi-directional, angular resolved scatterometry were used in order to evaluate the feasibility of rolled aluminium as reflectors in solar thermal collectors and solar cells. Two types of rolled aluminium with different surface roughness were investigated. The results show that the smoother of the two samples (rms height of  $(0.20 \pm 0.02)$   $\mu\text{m}$ ) can be used as a non-imaging, concentrating reflector with moderate reflection losses compared to optically smooth aluminium reflectors. The sample with the rougher surface (rms height  $(0.6 \pm 0.1)$   $\mu\text{m}$ ) is not suitable as a concentrating element but can be used as planar reflectors. The orientation of the rolling grooves is then of importance in order to minimise reflection losses in the system.

## Paper X Optical characterization of industrially sputtered nickel-nickel oxide solar selective surface

Tandem absorbers are often used in the design of solar absorbers for photo thermal conversion. They consist of a thin coating, selectively absorbing in the wavelength range of the solar spectrum, on a metal substrate. The optical performance of a tandem absorber depends on the optical constants and thickness of the absorbing coating and also the reflectivity of the underlying metal. A very high solar absorptance is achieved when the coating has a non-uniform composition in the sense that the refractive index is highest closest to the metal substrate and then gradually decreases towards the front surface. This type of composition suppresses coating interference and gives a low front surface reflection if also the refractive index at the front surface is low. We report on optical analysis of a solar absorber with a graded index coating of sputtered nickel/nickel oxide deposited on aluminium. The optical constants have been determined from reflectance, transmittance and ellipsometry data by fitting the data to a two-layer model of the coating. The optical constants of the two layers can be regarded as effective optical constants for the lower and upper part of the graded index coating respectively. It is found that the effective refractive index of the top layer is somewhat lower than for the base layer. The extinction coefficient is higher in the lower part of the coating. Both effective refractive index and extinction coefficient of the base layer increase monotonically with increasing wavelength as for metallic materials.

## 6 ACKNOWLEDGEMENTS

The work has been carried out under the auspices of The Energy Systems Programme, which is financed by the Swedish Foundation for Strategic Research, the Swedish Energy Agency and Swedish industry. Vattenfall Utveckling AB provided very important input to this work; supervision from their experienced staff and access to their solar collector laboratory.

During my years as a PhD-student I have been supported and supervised by a number of people that I would like to thank. Ewa Wäckelgård has been my main supervisor during the whole period. She has been an excellent supervisor and friend who has provided good comments and advise to my work as well as my personal questions. My co-supervisor has been Björn Karlsson from Vattenfall Utveckling AB. He has provided me with interesting projects and infected me with his MaReCo enthusiasm. If I add together all the hours that I have been waiting for him personally or for him to comment my work it would come to a lot of hours, but Björn is definitely worth waiting for. On a personal level I would also like to thank Björn for always being very considerate and frank. Arne Roos has made a tremendous work in correcting the English in all my publications and I consider him as my co-co-supervisor. He is also a very good travel mate and bought me colourful pills when I was feeling bad in Australia. During my work with flat-plate collectors I got a lot of help and advise from Bengt Perers at Vattenfall Utveckling AB. Thank you Claes-Göran Granqvist for being my professor and for signing all those letters of recommendation for my scholarship applications that made it possible for me to go to lots of interesting conferences.

In general the Solid State Physics group and the Ångström laboratory is full of nice persons providing the important social environment needed to do a good job, thank you all! I would especially like to thank the lunch gang for all these interesting lunch discussions during these years, AnnaKarin, Anna-Lena, Arne, Annette, Barbara, CG, Kristina, Maria, Richard, Solveig, Tobias and Tuquabo. CG is also a kind of sensible person on duty that gives advice in various areas, from physics to housebreaking. My ex-roommates Monica and Andreas are acknowledged for great discussions about life in general and food in particular. Monica and Maria are special friends that I appreciate very much. Fika is not the same without AnnaKarin. Kristina is a very good friend and sort of my “plastic little sister”. Annette is also a very good friend and advisor in spiritual and chemical matters. Joakim is my fellow energy systems PhD and we’ve had a lot of good talks on trains together. Life would not be the same without the e-mails with advice in various areas from Lisen. Thank you Tuquabo for introducing Eritrean food to me.

I would also like to acknowledge Anders Boulogner at the Communications Department for his expected and unexpected appearances at the lab and elsewhere. Ingrid Ringård is acknowledged for having the answers to all possible questions. Bengt H and Per are acknowledged for being good co-writers and keeping the spirit up even during late hours. Mats R is acknowledged for being a great person and for his

interesting work on concentrators. Normally acknowledgements are about the past, but I would also like to thank the new PhD-students at Solid State Physics for their enthusiasm that ensures that the traditions of the department will continue.

My husband Björn and my family are also entitled to an acknowledgement. Thank you Björn for loving me and taking care of me. I would also like to express my gratitude to my family for supporting me.

## 7 REFERENCES

- Benitez, P., Hernández, M., Mohedano, R., Miñano, J.C. and Muñoz, F. (1999) New nonimaging static concentrators for bifacial photovoltaic solar cells, in Proceedings of SPIE - The International Society for Optical Engineering: Nonimaging optics Vol 3781: Maximum efficiency light transfer V, Denver, Colorado, July 1999, pp. 22-29. ISSN 0277-786X.
- Born M. and Wolf E. (1980). Principles of optics, 6<sup>th</sup> edition, Pergamon, Oxford
- Chant, V.G., Håkansson, R., *The MINSUN simulation and optimisation program. Application and users guide.* IEA SH & C Task VII, Ottawa 1985
- Chaves, J. and Collares-Pereira M. (2000) Ultra flat ideal concentrators of high concentration, *Solar Energy* **69**, 269-281.
- Duffie J.A. and Beckman W.A. (1991). *Solar engineering of thermal processes*, 2<sup>nd</sup> edn. p 309. Wiley Interscience, New York
- Fendt T. and Wenzel K. (1999) Optical flux measurements in the focal area of a parabolic trough concentrator. *J. De Physique IV*, France Pr3-605
- Granqvist CG. (1991) Materials science for solar energy conversion systems, Pergamon Press, Oxford UK, ISBN 0-08-040937-7
- Hellström B. (2001) Parameter impact on temperature distribution and collector efficiency of a solar cell/collector hybrid in a CPC geometry. Internal Report Vattenfall Utveckling U 01:22, Älvkarleby, Sweden
- Hinterberger, H. and Winston R. (1966). *Review of Scientific Instruments*, **37**, 1094
- Karlsson B. and Wilson G. (1999) MaReCo- a large asymmetric CPC for high latitudes. Presented at ISES World Solar Congress 1999 Israel.
- McIntire W.R. and Reed K.A. (1983) Orientational relationships for optically non-symmetric solar collectors, *Solar Energy* **31**, 405-410
- Mills D.R. and Giutronich J.E. (1978) Asymmetrical non-imaging cylindrical solar concentrators, *Solar Energy* **20**, 45-55.
- Morrison G.L. (2001) Solar Collectors. In Solar energy the state of the art ISES position papers, Gordon J. (Ed) pp 145-219. James & James, London, UK.
- Nayak J.K. and Amer E.H. (2000) Experimental and theoretical evaluation of dynamic test procedures for solar flat-plate collectors. *Solar Energy* **69**(5) pp. 377-401.

Nordlander S. and Rönnelid M. (2001). Load adapted collectors for high solar fractions. In proceedings of North Sun Conference 6-8 May, Leiden, The Netherlands.

Nordling C. and Österman J. (1987). Physics Handbook, Studentlitteratur, Lund, Sweden ISBN 91-44-16574-9

Nostell P, Roos A and Karlsson B (1997) Optical characterisation of solar reflecting surfaces. *In proceedings of SPIE*, paper 3138-20 (1997), pp. 163-172, San Diego, USA

Nostell P, Roos A and Karlsson B (1998) Ageing of solar booster reflector materials. *J. Solar Energy Materials and Solar Cells* **54**, pp 235-246

Nostell P, Roos A and Karlsson B (1999) Optical and mechanical properties of sol-gel antireflective films for solar energy applications. *J Thin solid films* **351**, 170-175

Perers B. and Walletun H. (1991) Dynamic collector models for 1 h time step derived from measured outdoor data. In proceedings ISES Solar World Congress, 19-23 August, Denver, USA, Vol.2, Arlen M.E., Burley M. and Coleman S. M. A. (Eds.), pp. 1221-1226, Pergamon Press, New York.

Perers B. (1993a) Dynamic method for solar collector array testing and evaluation with standard database and simulation programs. *Solar Energy*, **50**(6) pp 517-526.

Perers B. and Karlsson B. (1993b) External reflectors for large solar collector arrays, simulation model and experimental results. *Solar Energy*, **51**(5), 327-337.

Perers B., Karlsson B. and Bergkvist M. (1994). Intensity distribution in the collector plane from structured booster reflectors with rolling grooves and corrugation. *Solar Energy* **53**, 215-226.

Perers B. (1995) Optical modelling of solar collectors and booster reflectors under non stationary conditions, thesis Uppsala University 1995.

B. Perers (1997) An improved dynamic solar collector test method for determination of non-linear optical and thermal characteristics with multiple regression. *Solar Energy* **59** (4-6) pp. 163-178.

Pinazo J.M., Canada J. and Arago F. (1992). Analysis of the incidence angle of the beam radiation on CPC. *J. Solar Energy* **49**, 175-179.

Rabl, A. (1976). Comparison of solar collectors, *Solar Energy* **18**, 93

Roos A. (1997) Optical characterisation of coated glazings at oblique angles of incidence: measurements versus model calculations. *Journal of Non-Chrystalline solids* **218**, 247-255

Rönnelid M. and Karlsson B. (1996). Experimental investigation of heat losses from low-concentrating non-imaging concentrators. *Solar Energy* **57**, 93-109

Rönnelid M., Karlsson B. and Gordon J.M. (1996). The impact of high latitudes on the optical design of solar systems. In *Proc. Euro '96*, Freiburg, Germany, September 16-19

Rönnelid M. and Karlsson B. (1997). Radiation distribution diagrams and their use for estimating collectable energy. *Solar Energy* **61**, 191-201.

Rönnelid M. and Karlsson B. (1998). Optical properties of modified compound parabolic concentrators with linear corrugated reflectors. *Appl. Opt.* **37**, 5222-5226

Rönnelid M. and Karlsson B. (1999). The use of corrugated booster reflectors for large solar collector fields. *Solar Energy* **65**, 343-351

Rönnow D and Veszelei E (1994). Design review of an instrument for spectroscopic total integrated light scattering measurements in the visible wavelength region. *Rev. Sci. Instrum.* **65**, 327-334

Rönnow D (1997). Determination of interface roughness correlations of thin films from spectroscopic light scattering measurements. *J. Appl. Phys.* **81**, 3627-3636.

Smyth, M., Zacharopoulos, A., Eames, P.C. and Norton B. (1999). An experimental procedure to determine solar energy flux distributions on the absorber on line-axis compound parabolic concentrators. *Renewable Energy* Vol. **16** pp 761-764

Tripanagnostopoulos Y., Yianoulis P., Papaefthimiou S., Souliotis M. and Nousia Th. (1999) Cost effective asymmetric CPC solar collectors. *J. Renewable Energy* **16**, 628-631

Tripanagnostopoulos Y., Yianoulis P., Papaefthimiou S. and Zafeiratos S. (2000) CPC solar collectors with flat bifacial absorbers. *J. Solar Energy* **69**, 191-203

Wittver V and Platzer W. (1990). Transparent Insulation Materials. *In proceedings of SPIE 1990*, Haag

Wangsness, R.K. (1986) *Electromagnetic fields*, J Wiley & Sons, New York, ISBN 0-471-85912-5

Welford W.T. and Winston R. (1989) *High collection non-imaging optics*, Academic Press, San Diego ISBN 0-12-742885-2

Winston R (2001) *Solar Concentrators*. In *Solar energy the state of the art ISES position papers*, Gordon J. (Ed) pp 357 -436. James & James, London, UK.

Wäckelgård E. and Hultmark G. (1998) Industrially sputtered solar absorber surface. *Solar Energy Materials and Solar Cells* **54**, 165-170

Wäckelgård E., Niklasson G. and Granqvist C.G. (2001) Selectively solar-absorbing coatings. In *Solar energy the state of the art ISES position papers*, Gordon J. (Ed) pp 109-144. James & James, London, UK.